Aryl hydrocarbon receptor restricts axon regeneration of DRG neurons in response to injury

Yiqun Wang [1,2*], Dalia Halawani [1*#], Molly Estill [1], Aarthi Ramakrishnan [1], Li Shen [1], Roland H. Friedel [1,3], Hongyan Zou [1,3,#]

[1] Nash Family Department of Neuroscience, Friedman Brain Institute, Icahn School of Medicine at Mount Sinai, New York, USA

[2] Current address: Sport Medicine Center, Honghui Hospital, Xi'an Jiaotong University, Xi'an, China

[3] Department of Neurosurgery, Icahn School of Medicine at Mount Sinai, New York, USA

*Equal Contribution

Corresponding authors: dalia.halawani@mssm.edu, hongyan.zou@mssm.edu

Abstract

Injured neurons sense environmental cues to balance neural protection and axon regeneration, but the mechanisms are unclear. Here, we unveil aryl hydrocarbon receptor (AhR), a ligand-activated bHLH-PAS transcription factor, as molecular sensor and key regulator of acute stress response at the expense of axon regeneration. We demonstrate responsiveness of DRG sensory neurons to ligand-mediated AhR signaling, which functions to inhibit axon regeneration. *Ahr* deletion mimics the conditioning lesion in priming DRG to initiate axonogenesis gene programs; upon peripheral axotomy, *Ahr* ablation suppresses inflammation and stress signaling while augmenting pro-growth pathways. Moreover, comparative transcriptomics revealed signaling interactions between AhR and HIF-1α, two structurally related bHLH-PAS α units that share the dimerization partner Arnt/HIF-1β. Functional assays showed that the growth advantage of AhR-deficient DRG neurons requires HIF-1α; but in the absence of Arnt, DRG neurons can still mount a regenerative response. We further unveil a link between bHLH-PAS transcription factors and DNA hydroxymethylation in response to peripheral axotomy, while neuronal single cell RNA-seq analysis revealed a link of the AhR regulon to RNA polymerase III regulation and integrated stress response (ISR). Altogether, AhR activation favors stress coping and inflammation at the expense of axon regeneration; targeting AhR can enhance nerve repair.

Key words:

Aryl hydrocarbon receptor (AhR), Axon regeneration, Conditioning lesion of DRG, Hypoxia-inducible factor (HIF), Arnt, DNA hydroxymethylation, Integrated stress response (ISR)

Introduction

Injured neurons experience alteration of their environment due to inflammation, tissue damage, change in microbial populations or oxygen tension. Safeguard mechanisms have evolved to allow injured neurons to sense external cues to cope with stress, adjust metabolism or synaptic transmission, and launch regenerative gene programs. Timely execution of these tasks requires precise transcriptional rewiring, but the underlying mechanisms remain opaque.

The basic helix-loop-helix/PER-ARNT-SIM (bHLH-PAS) transcription factors (TFs) have evolved for molecular sensing of physiological and environmental cues, e.g., circadian activity, hypoxia, and xenobiotic exposure [1,2]. A recent study from our laboratory has uncovered a role of Bmal1, a core circadian regulator, in gating regenerative responses of dorsal root ganglia (DRG) sensory neurons after peripheral axotomy [3]. Hypoxia-inducible factor (HIF)-1α activation through intermittent hypoxia has been shown to promote axon regeneration of DRG neurons [4]. Aryl hydrocarbon receptor (AhR) and HIF-1α are two structurally related α units of bHLH-PAS TFs that share the dimerization partner aryl hydrocarbon receptor translocator (Arnt), a.k.a. HIF-1β. The function of AhR or Arnt in the setting of axotomy and their signaling relationship with HIF or Bmal1 have not been studied.

Initially characterized as a molecular sensor of environmental toxins such as dioxin, AhR is the only ligand-activated bHLH-PAS TF that can bind to a broad spectrum of dietary, microbial, and metabolic compounds [5]. Ligand binding triggers nuclear translocation of AhR and subsequent dimerization with Arnt (also known as HIF-1β) to initiate context-specific transcriptional responses by binding to AhR response elements (AHRE; also termed xenobiotic response elements (XRE) or dioxin response elements (DRE)) [6]. One hallmark of canonical AhR signaling is the AHRE-controlled induction of cytochrome P450 enzymes for detoxification (i.e., Cyp1a1, Cyp1a2, and Cyp1b), as well as NRF2-dependent anti-oxidation genes [7,8]. AhR signaling is tightly controlled, as Cyp1 enzymes metabolize

AhR ligands; their induction thus constitutes inhibitory feedback to terminate AhR activity [9]. AhR activation also induces its own repressor, the AhR repressor (AhRR) [10], which not only dimerizes with Arnt and competes for AHRE occupancy, but also inhibits AHRE-mediated transcription through chromatin reconfiguration around the promoter of AHRE-driven genes [11]. The presence of multiple feedback inhibition mechanisms underscores the physiological importance of avoiding toxicity from prolonged AhR signaling [6].

Another mechanism that restricts AhR activity is the competition with HIF-1α for Arnt [12,13], but the antagonistic competition between AhR and HIF-1α is highly context-dependent [14-16], and in some scenarios they may act cooperatively [16] or even synergistically for gene regulation [17] . Recent study from the Quintana laboratory has also revealed a temporally controlled access to Arnt, with HIF-1α acting first and then AhR taking over, adding further complexity of the crosstalk [16].

Previous studies on AhR have largely focused on toxicology, barrier tissue integrity, and immunology, less is understood of its function in axon regeneration and interplay with HIF-1α or Arnt. Here, we took advantage of a unique feature of DRG neurons wherein peripheral axotomy (conditioning lesion) triggers regeneration of not only peripheral but also central axonal branches [18,19]. We showed responsiveness of DRG neurons to ligand-mediated AhR signaling. Functional assays with AhR agonists/antagonists and conditional gene deletion demonstrated that AhR functions to inhibit axon regeneration. We further defined AhR injury regulon and the signaling relationships with HIF-1α and Arnt in balancing stress coping and axon regeneration. Neuronal single cell RNA-seq analysis uncovered a link of AhR regulon with RNA polymerase III regulation and integrated stress response (ISR). These new understandings will help advance neural repair strategies.

Results

DRG neurons display responsiveness to ligand-mediated AhR signaling

To understand transcriptional mechanisms in response to axotomy, we analyzed a set of early response TFs that we had identified in axotomized DRG at 12 or 24 hr after peripheral lesion (PL, regenerative) as compared to central lesion CL, non-regenerative) [20]. These included well-known regeneration-associated TFs such as ATF3 [21], Sox11 [22], Jun [23], Smad1 [20,24], ATF4 [25], and early response genes (ERG) such as EGR1 and CREM, as well as AhR. STRING analysis [26] revealed an interconnected network of these TFs but no known functional connection with AhR (**Fig. 1a**). This also applied to a larger set of 39 TFs predicted to be linked to axon regeneration [27], showing interconnection between Smad, Fos, Stat, and Jun, but no known connection with AhR (**Fig. S1a**).

As AhR is the only ligand-activated bHLH-PAS TF, we first assessed responsiveness of primary adult DRG neurons to AhR agonists – ITE, an indole-derived dietary compound and a physiological ligand of AhR with many disease modulatory roles [28-30], and L-kynurenine (L-Kyn), a tryptophan metabolite –, or a ligand-selective antagonist CH-223191 (CH) [31] (**Fig. 1b**). Immunocytochemistry (ICC) revealed nuclear translocation of AhR by ITE and L-Kyn, and cytoplasmic retention by CH (**Fig. 1c**). Notably, primary DRG neurons maintained in serum-free defined media exhibited baseline nuclear AhR immunosignals at 26 hr after plating, signifying the presence of endogenous AhR ligands.

As a direct readout of AhR transcriptional activity, we next examined the expression of *Cyp1a1* and *Cyp1b1,* two canonical AhR target genes in the detoxification pathway, as well as *Ahrr*, a bHLH-PAS TF acting in a negative feedback loop. qRT-PCR demonstrated the expected induction or suppression of these AhR target genes by agonists or antagonist, respectively (**Fig. 1d**). In congruence, in vivo administration of ITE (i.p. injections over 3 days) also induced *Cyp1a1, Cyp1b1* expression, and a trend for increase of *Ahrr* expression in DRG, as shown by qRT-PCR or Western blots (WB) (**Fig. 1e, f**).

Notably, WB also revealed an electrophoretic mobility shift of AhR, reflecting post-translational modifications upon ligand stimulation.

Surveying a human tissue gene expression atlas revealed high expression of *AHR* in peripheral nerve as compared to brain or other non-neural tissues in both female and male, hinting a unique role of AhR for nerve physiology (**Fig. S2a**). Analysis of single cell RNA-sequencing (scRNA-seq) data of mouse nervous system [32] further revealed expression of *Ahr, Hif1a,* and *Arnt* in a variety of CNS and PNS neurons, including DRG neurons, and a particularly high expression of *Cyp1b1* in peptidergic DRG neuron subtypes (**Fig. S2b**). Together these initial data illustrate responsiveness of DRG neurons to ligand-mediated AhR signaling.

AhR activation inhibits neurite outgrowth

To probe the functional significance of AhR signaling for neurite outgrowth, we first tested the effect of AhR agonist or antagonist on neurite outgrowth of induced neurons derived from human embryonic stem cells (**Fig. 1g**). Interestingly, application of AhR agonist Norisoboldine led to shorter neurites, whereas the antagonist CH resulted in longer neurites (**Fig. 1g**). These results were confirmed in a larger screen demonstrating a growth promoting effect of AhR antagonists CH or TMF (in a dose-dependent manner), and StemRegenin 1 (**Fig. S1b**).

Similar axon growth prompting or inhibitory effects of AhR antagonist or agonist were also obtained with primary adult DRG neurons, albeit with some variability, perhaps reflecting batch variation of endogenous AhR ligands (**Fig. S1c**). Notably, the growth inhibitory effect of AhR agonist was only observed in cultured DRG neurons with continuous exposure to ITE, but not in those with transient in vivo exposure to ITE 1 to 2 days prior to dissociation (**Fig. S1d**). Collectively, these results aligned with context-dependent effects of AhR ligands and the transient nature of AhR signaling due to multiple

negative feedback mechanisms [6].

To corroborate our finding of an inhibitory role of AhR on axon growth, we generated *Ahr* conditional knockout (cKO) mice by breeding $Ahr^{fl/fl}$ with $Nestin^{Cre}$ allele [33,34] (**Fig. 2a**). WB confirmed reduced AhR levels in both brain and DRG tissues from cKO mice relative to littermate controls (**Fig. 2b**). WB also showed that PL led to upregulation of AhR, but only in control and not Ahr^{cKO} DRG (**Fig. 2c).**

While constitutive *Ahr* deletion results in demyelinating disease and inflammation [35,36], the *Ahr* cKO $^{Nes\text{-}Cre}$ mice appeared healthy and fertile with no overt motosensory deficits. We next performed crush injury on sciatic nerve and examined sensory axon regeneration by IF for SCG10, a marker that specifically labels regenerating but not uninjured sensory axons [37] (**Fig. 2d, e**). Consistent with the results from AhR antagonists, *Ahr* deletion also promoted axon regeneration, with more and longer $SCG10^{+}$ axons extending beyond the crush site at 2 day post injury (dpi), as measured by regenerative index and maximal axonal length (1.44 mm vs. 1.06 mm, a 36% increase) (**Fig. 2f**).

Neuron specific *Ahr* ablation enhances axonal regeneration

For further confirmation of our findings, we also generated *Ahr* cKO^{CreER} mice for time-controlled neuron-specific deletion of *Ahr* by breeding $Ahr^{fl/fl}$ with Thy1-$Cre^{ERT2/EYFP}$ (SLICK-H) mice [38,39]. As the Thy1-$Cre^{ERT2/EYFP}$ transgene utilizes a bidirectional *Thy1* promoter to drive neuronal expression of tamoxifen-inducible Cre^{ERT2} and EYFP, we first verified expression of EYFP in DRG neurons (**Fig. S3a**). We also crossed Thy1-$Cre^{ERT2/EYFP}$ to a reporter line (Rosa26-LSL-Sun1-GFP) [40] to further confirm tagging of DRG neurons upon tamoxifen injection (**Fig. S3b, c**). Genotyping verified excision of the *Ahr* floxed allele in DRG but not tail tissues from the cKO mice at 2 weeks after tamoxifen injection (**Fig. S3d, e**), while RNA-seq showed reduced mRNA reads of *Ahr* exon 2 (floxed region) in Ahr^{cKO} DRG samples relative to controls (**Fig. S3f**).

We next evaluated motosensory performance of adult *Ahr* cKO^{CreER} mice and littermate controls at 2 or 5 weeks after tamoxifen administration, which displayed comparable performance for ladder walking with regular or irregular intervals and tactile perception by Von Frey filament testing (**Fig. S4a-c, Supplementary Video S1, S2**). Hence, induced neuronal AhR ablation in adult mice did not appear to impair physiological nerve function in the time frames tested.

In congruence with the results from Nestin-Cre driven *Ahr* cKO and AhR antagonists, neurite outgrowth assay showed that DRG neurons from *Ahr* cKO^{CreER} mice also extended longer neurites at 24 hr post-seeding (mean length of 393 vs. 232 μm, a 70% increase) (**Fig. 3b, c**). The increased neurite length of *Ahr*-deficient DRG neurons did not reach that of conditioned DRG neurons (**Fig. 3c**), indicating that the conditioning lesion also operates through AhR-independent mechanisms.

The enhanced axon regeneration phenotype with *Ahr* cKO also held true for the in vivo sciatic nerve injury model, with more and longer SCG10^{+} regenerating axons extending beyond the crush site at both 1 dpi (longest axon length 869 vs. 594 μm, ~ 50% increase) and 3 dpi (5.8 vs. 4.8 mm, ~ 20% increase) (**Fig. 3d-h**). The regenerative phenotype at these early time points supports a priming effect of *Ahr* deletion for early initiation of regeneration gene programs.

We further conducted motosensory behavioral assays, which showed accelerated functional recovery of *Ahr* cKO mice relative to controls (**Fig. 3i-k**). At baseline, both genotypes displayed similar ability to fully spread toes in hindlimb, and sciatic nerve crush injury resulted in pronounced toe flexing and failure to bare weight on injured hindlimb in both cohorts. But by 9 dpi and also at 13 and 17 dpi, *Ahr* cKO mice exhibited improved hindlimb toe spreading, reflected by sciatic functional index (SFI). Together,

these results illustrated AhR as an inhibitor of axon regeneration; AhR deletion accelerated axon regrowth and functional recovery after peripheral nerve injury.

PL triggers an early induction of bHLH-PAS transcription factors in axotomized DRG

To better understand AhR signaling in conditioning lesion of DRG (enhanced axon regeneration capability [18,19]), we profiled DRG transcriptomic by RNA-seq, which revealed a positive enrichment for both Xenobiotic metabolism and Hypoxia gene sets at 1 dpi after PL relative to naive DRG (**Fig. 4a, b, Table S1**). Consistently, RNA-seq revealed increased mRNA reads for both *Ahr* and *Hif1a* at 1 dpi (**Fig. 4c**). Time-course qRT-PCR analyses verified an early induction of *Ahr* and *Arnt* at 12 hr post-PL, which persisted at 48 hr; by comparison, *Hif1a* induction lagged slightly behind and was more transient, peaking at 24 hr and returning to baseline by 48 hr (**Fig. 4d**). In echo, analysis of a recent scRNA-seq dataset on conditioned DRG [41] also confirmed early induction of the three bHLH-PAS TFs (*Ahr, Hif1a, Arnt)* in majority of DRG neuron subtypes from 12 to 72 hr post-PL (**Fig. S5a**).

Early induction of AhR in DRG after PL was also demonstrated by WB: detectable as early as 2 hr, further increasing by 12 hr, peaking at 1-3 dpi, and persisting at 14 dpi. This pattern paralleled that of ATF3, a marker of the conditioning lesion [21] (**Fig. 4e, f**). HIF-1α induction/stabilization after PL also occurred early but appeared more transient: detectable at 12 hr (slightly preceding transcriptional changes), peaking at 1 dpi, but returning to baseline by 3 dpi (**Fig. 4e, f**).

As another sign of AhR activation, Cyp1b1 displayed an early but transient upregulation at 1 to 3 dpi after PL, shown by WB, RNA-seq, and qRT-PCR time-course analyses, and the same result was also observed for *Tiparp* (TCDD inducible poly(ADP-ribose) polymerase), another AhR target gene and a negative regulator of Ahr activity [42] (**Fig. 4e-g**, **S5b**). *Cyp1a1* and *Ahrr* had low expression in DRG. It was notable that AhR displayed an electrophoretic mobility shift after PL, particularly at 12 and 24 hr,

similar to that by AhR agonist (**Fig. 4e**, also observed in **Fig. 1f**). Hence, conditioning lesion seems to trigger only a transient AhR activation by endogenous ligands despite persistent elevation of AhR expression, in line with multiple feedback mechanisms to swiftly turn off AhR signaling [6].

AhR stability/cytoplasmic retention is controlled by cytoplasmic chaperones HSP90, XAP2 (AhR interacting protein, *Aip*), and p23 (Prostaglandin E Synthase, *Ptges3*) (**Fig. S6a**). RNA-seq showed that PL led to downregulation of *Aip* but not *Ptgs3* or *Hsp90* at 1 dpi, while qRT-PCR showed a downregulation of both *Aip* and *Ptgs3* at 36 hr (**Fig. S6b, c, Table S1**). These changes support an early AhR activation after PL. Attempts of IHC for AhR in DRG tissues did not yield specific immunosignals, thus precluding in vivo assessment of AhR nuclear localization.

Ahr activation can be controlled by L-kynurenin metabolic pathway [43], we thus examined the expression of six biosynthesis enzymes involved in the conversion of tryptophan to L-Kyn or kynurenic acid, all showing no overt changes at 1 dpi by RNA-seq (**Fig. S6d, e**). Time course qRT-PCR analysis revealed a downregulation of *Kyat1* but not *Kmo* at 36 hr, while an earlier gene matrix analysis [44] revealed a modest downregulation of *Tdo2* at 3 dpi after PL, and low expression of *Ido1* and *Ido2* in DRG (**Fig. S6f, g**). Hence potential alterations of endogenous AhR ligands in response to axotomy likely originate from sources outside of DRGs. Altogether, concurrent early induction of AhR and HIF-1α after axotomy likely set the stage for collaboration or competition to balance stress coping vs. regeneration (**Fig. 4h**).

Predicted AHRE and HRE-driven RAGs engage common and distinct pathways for metabolism, stress response, and axonogenesis

Given the transcriptional roles of AhR and HIF-1α, we applied ChEA3, an integrative TF enrichment analysis tool that combines ChIP-seq datasets, gene co-expression, and TF-gene co-occurrence [45] on regeneration-associated genes (RAGs) identified by our RNA-seq in conditioned DRG at 1 dpi relative

to naive state (n=3,022; cutoff: $\log_2$FC 0.25 and P<0.01) (**Fig. S7a, S8a**). This revealed 432 (14%) AhR-associated RAGs including ATF3 and Jun (**Fig. S7b, Table S2**), and 268 of them harbored AHRE in their promoter (**Fig. S7c**). In comparison, ChEA3 identified 385 (13%) HIF-1α-associated RAGs, also including ATF3 and Jun, as well as Gadd45a and IL6, and 144 of them harbored HRE in their promoter (**Fig. S8a-c, Table S3**).

IPA of enriched pathways and graphic summary revealed that the RAGs associated with AhR and HIF-1α engaged shared but also distinct pathways related to acute stress response and axonogenesis. For instance, the 432 AhR-associated RAGs concerned xenobiotic metabolism (confirming AhR association), HIF signaling (signifying a connection between AhR and HIF), axonogenesis (e.g., Axon guidance, PTEN inhibition, ERK/MAPK), metabolism (Thyroid hormone receptor/Retinoid X receptor (TR/RXR), stress responses (Acute phase response, Glucocorticoid receptor signaling, Unfolded Protein Response, Phagosome formation, NRF2-mediated oxidative stress response, Wound healing), and immune trafficking (IL6, Sphingosine-1 phosphate) (**Fig. S7d, e**). By comparison, the 385 HIF-1α-linked RAGs mainly concerned Hypoxia, Creatin metabolism, Circadian, Axon guidance Plexin D1, and BDNF signaling (**Fig. S8d, e**). There were 142 common genes linked to both AhR and HIF-1α (**Fig. S8g, Table S4**). Surveying a time-course gene matrix analysis of conditioned DRG [44] revealed that the majority of the RAGs linked to AhR, HIF-1α, or both were upregulated from 1 to 14 dpi (**Fig. S7f; S8f, h, Table S5 to S7**).

AhR-dependent genes favor acute stress and inflammation at the expense of axonogenesis

To further define the AhR regulon, we performed RNA-seq analysis on DRG from control and *Ahr* cKO^{CreER} mice in naive state or after PL at 1 dpi (**Fig. 5a**). This revealed 253 *Ahr* cKO DEGs in naive DRG (115 up- and 138 down-regulated), and 189 DEGs in PL axotomized DRG (73 up- and 116 down-regulated) (**Fig. 5b, c, S9a, b, Table S8, S9**).

For the 253 DEGs in naive DRG, 156 (62%) harbored AHRE in their promoter, with majority (83%) being downregulated in cKO (likely direct targets of AhR). Interestingly, 59 DEGs (23%) harbored HRE in their promoter, and all of them also harbored AHRE (dually regulated by AhR and HIF-1α) (**Fig. S9c**). Of the 189 DEGs in axotomized DRG, 80 (42%) contained promoter AHRE, 16 (8.5%) HRE, and 27 (14%) both, while 66 (37%) had no motif (**Fig. S9d**).

Pathway analysis by Enrichr revealed that the downregulated DEGs in both naive and axotomized *Ahr*^{cKO} DRG were enriched for inflammation, albeit involving different pathways, e.g., interferon (IFN) and chemokines featured in naive cKO DRG, and complement and TNF in axotomized DRG (**Fig. 5d**, **e**). The upregulated DEGs in both states mainly concerned neuronal functions (e.g., voltage-gated Ca^{2+} and K^+ channels), with synapse organization and axonogenesis featured in naive cKO DRG, while G protein coupled receptor (GPCR) and carbohydrate biosynthesis featured in axotomized cKO DRG (**Fig. 5d, e**).

IPA further highlighted immune suppression and reduced stress as the main biological themes of *Ahr* ablation in both DRG conditions, with tryptophan degradation (confirming AhR regulation) and axonogenesis featured in naive state, while HIF-1α signaling (a link between AhR and HIF) and carbohydrate metabolism featured in axotomized state (**Fig. S9e-h**). Concordantly, GSEA showed that transcriptomes of naive and axotomized *Ahr*^{cKO} DRG share common negative enrichment for inflammation, Hypoxia, and ROS, and positive enrichment for Hedgehog signaling, but also distinct gene set enrichment (**Fig. S10, Table S10**).

Ahr deletion leads to a priming effect mimicking the conditioning lesion

As axonogenesis pathways were enriched in *Ahr*^{cKO} DRG, we next asked whether AhR ablation mimics the conditioning lesion in initiating regenerative gene programs. To this end, we intersected the 235 cKO

DEGs of naive DRG with the 3,022 RAGs induced by PL (conditioning lesion) at 1dpi, revealing 61 overlapping genes (25%) that concerned Axonal extension, DNA binding/transcription (e.g., DNA unwinding, TFIIH core complex, 3'-5' DNA helicase activity, Double stranded DNA binding), Negative regulation of Wnt signaling (pro-axon regeneration [46,47]), as well as Retinoid metabolic process and Phospholipase activity (**Fig. 5f, S11a, Table S11**). Heatmap highlighted that transcriptional changes of 10 RAGs in the GO terms related to axonogenesis (e.g., *Klf8*, *Ncam1, Hoxd11, Hoxc8*) as a result of *Ahr* ablation mimicked that of conditioning lesion (**Fig. 5g**).

Notably, RNA-seq and qRT-PCR showed that *Ahr* deletion did not induce well-known RAGs in naive DRG, nor altering PL-triggered transcription changes of these RAGs, e.g., *Atf3, Smad1*, neurotrophins (*Bdnf, Ngf, Ntf3*), or canonical HIF pathway genes (*Hif1a, Vegfa, Slc2a1*) (**Fig. S11b, c**). This also applied to *Ppargc1a* (a master regulator of mitochondrial, glucose and fatty acid energy metabolism) [48-50]. IF validated no overt changes of GAP43, pCREB, or ATF3 in naive Ahr^{cKO} DRG neurons, except for a modest elevation of pSmad1/5/8 relative to control (**Fig. S11d**).

Since ATF3 was a top RAG associated with both AhR and HIF-1α (predicted by ChEA3 analysis), and it contains AHRE in its promoter (**Fig. S12a,** refer to Table S2), we further assessed the impact of *Ahr* ablation on ATF3 expression. WB revealed that *Ahr* cKO did not alter the low baseline expression of ATF3 or its robust induction after PL (**Fig. S12b**), consistent with IF results (**Fig. S11d, S12c**). Altogether, ablation of AhR in DRG mimics the conditioning lesion in launching axon regenerative gene programs, involving novel gene pathways independent of ATF3.

We also examined the effects of in vivo administration of AhR agonist ITE, which induced genes containing AHRE in their promoter (*Atf3, Bdnf*, *Cyp1a1, Cyp1b1*), but not genes without AHRE (*Sprr1a, Gal, Npy, Csf1*) in naive DRG (**Fig. S12d,** refer to Table S2). IF showed that in vivo administration of

AhR antagonist TMF resulted in higher pSmad1/5/8 and pS6K$^{Ser235/236}$ in naive DRG neurons, consistent with higher axon growth potential (**Fig. S12f, g**). By contrast, TMF did not cause change of ATF3 expression, while ITE led to higher cytoplasmic ATF3 (**Fig. S12e**).

AhR ablation exerts distinct influence on DRG transcriptome in naive vs. axotomized state

We next focused on the impact of *Ahr* ablation on gene expression in DRG after PL. Intersection of 3,022 PL-RAGs with 189 cKO DEGs at 1 dpi revealed 49 common genes (AhR-dependent RAGs) concerning neuronal functions (e.g., Synapse long term depression, CREB signaling in neurons, Glutamate receptor signaling, Neurovascular coupling) and Phagosome Formation (**Fig. 5h, Table S12**). By contrast, the 140 unique AhR-dependent genes mainly concerned inflammation, lipid, ECM, and HIF-1α signaling (**Fig. 5h**). Heatmap comparison illustrated a profound impact of *Ahr* ablation on the expression of phagosome-associated genes for both shared and unique categories (**Fig. 5i**), suggesting a function of AhR via phagosome formation.

The striking transcriptional impact of *Ahr* ablation was also illustrated on the 23 RAGs showing progressive expression changes of from 3 to 14 dpi [44] (**Fig. S13a**). We also analyzed the predicted upstream regulators of the 189 DEGs in axotomized *Ahr*^{cKO} DRG by IPA, which revealed regulators related to immune response (e.g., IRF2BP2, MALT1, IL17RA), metabolism (SRF, TCL1A, FOXO1), vascular regulation (AGT), and growth factor signaling (EGF, TGFA) (**Fig. S13b**). These results support collaboration of AhR with diverse regulators in rewiring transcriptional networks.

While many similar pathways, particularly immune and stress response were enriched in both naive and axotomized *Ahr*^{cKO} DRG, the DEGs shared only 7 common genes (i.e., core AhR-regulated genes) that regulate sugar and amino acid metabolism (Glutamine-fructose-6-phosphate transaminase 2 (*GFPT2*),

Bisphosphoglycerate mutase (*BPGM*), immunity (Thy1; Immunoglobulin heavy constant gamma 3, *IGHG3*), secretion (Calcium dependent secretion activator or *CADPS*), or epithelial tube formation (Multimerin 2 or MMRN2), WD repeat domain 72 (WDR72) (**Fig. 5j**).

It is also noteworthy that even though inflammatory suppression was a main biological theme in *Ahr*-deficient DRG, IF showed no overt changes for IBA1, a marker of myeloid cells, or CD45, a pan leukocyte marker, in naive or axotomized DRG (**Fig. S13c-e**). Hence the impact of AhR ablation on inflammatory suppression was not simply reflected by changes in the abundance of immune cells.

To further understand the differences between the AhR regulons in naive vs. axotomized DRG, we conducted comparative IPA, which revealed that in the axon injury setting, *Ahr* deletion resulted in a wide suppression of neuroinflammation, neuronal function, and metabolic signaling, with the exception of neurovascular coupling and lipid synthesis (LXR/RXR activation) (**Fig. S14a**).

To assess the impact of *Ahr* ablation on transcriptomes of injured DRG, we also conducted comparative IPA on the PL-induced RAGs in control DRG (n=3,022) vs. Ahr^{cKO} DRG (n=3,183) (**Fig. S14b, Table S1, S13**). This comparison again underscored that *Ahr* ablation resulted in a general suppression of signaling related to stress response, immune, synaptic function, but also notably an augmentation of axon regenerative pathways such as GADD45, HIPPO, p53, DNA damage-induced 14-3-3 signaling (**Fig. S14b**). Hence, *Ahr* ablation exerted context-dependent transcriptional effects in naive vs. axotomized DRG.

Axon growth promoting effect of AhR ablation requires HIF-1α

Since AhR ablation is expected to increase availability of the heterodimerization partner Arnt for HIF-1α, we expected an enhancement of HIF signaling by *Ahr* deletion. However, while GSEA revealed that

PL led to a positive enrichment of Hypoxia gene set in both control and *Ahr*^{cKO} DRG, the ablation of AhR resulted in fact in an overall negative enrichment of Hypoxia gene set in both naive and axotomized DRG (**Fig. S15a**), a finding also observed by comparative IPA (see **Fig. S14a**).

We further examined 196 genes in the Hallmark_Hypoxia gene set, and hierarchical clustering revealed a complex transcriptional pattern on the level of individual genes, with many downregulated after PL (even though the Hypoxia gene set was enriched) (**Fig. S15b, Table S14**). PL clearly exerted a stronger effect on these genes, with only a modulatory effect from *Ahr* deletion (**Fig. S15b**). Venn diagram revealed only 2 and 3 overlapping genes between Hallmark_Hypoxia genes and *Ahr* cKO DEGs in naive or axotomized DRG, respectively (**Fig. S15c**). The same also applied to the HIF-1α dependent signature genes identified by Cho et al. [4] (n=495, of which 108 (22%) overlapped with the PL-RAGs) (**Fig. S15d, Table S15**), or the predicted HIF-associated RAGs (**Fig. S15e, f**). Taken together, *Ahr* deletion led to an overall suppression of HIF signaling, suggesting collaboration rather than antagonism of the two in the setting of axonal injury.

We next focused on functional relationship of AhR and HIF signaling. To this end, we treated DRG neurons with KC2F7, a specific inhibitor of HIF-1α protein synthesis via pS6K inhibition [51]. This resulted in a reversal of the axon promoting phenotype of *Ahr* deletion, without diminishing the outgrowth capacity of control neurons (**Fig. 6a-c**). We next tested DRG neurons that were conditioned by PL 3 days prior, which exhibited enhanced axon growth potential, with mean longest neurite length reaching 274 µm by 12 hr after plating. Remarkably, *Ahr* deletion further augmented the conditioning effect (with longest neurites reaching mean length of 326 µm, a 20% increase), and this was again diminished with KC2F7 treatment (**Fig. 6d-f**). In aggregate, the growth advantage of AhR-deficient DRG neurons seemed to require HIF-1α.

Absence of Arnt does not affect axon regrowth capacity of DRG neurons

Arnt is a common β unit for both AhR and HIF-1α. Since both Xenobiotic metabolism and Hypoxia gene sets were enriched in DRG after PL, we next tested the impact of simultaneous inactivation of AhR and HIF-1α pathways by *Arnt* cKO (*Arnt*$^{fl/fl}$ Thy1-Cre$^{ERT2/EYFP}$, confirmed by qRT-PCR) (**Fig. S16a**). Neurite outgrowth assays showed that *Arnt*-deficient DRG neurons extended axons of comparable length as controls (**Fig. 6g-i**), with no further effect from HIF inhibition by KC2F7 or HIF activation by hypoxia exposure (**Fig. S16b**). Likewise, conditioned neurons exhibited similar axonal length regardless of genotype or oxygen tension (**Fig. 6h, i, S16c**).

In line with the in vitro data, sciatic nerve in vivo injury experiments also showed that the extent of regenerating axons (SCG10^{+}) in *Arnt* mutant mice matched that in littermate controls at 3 dpi (maximal mean length 4.6 ± 0.3 vs. 4.7 ± 0.4 mm) (**Fig. 6j-l**). These data indicated that in the absence of Arnt, DRG neurons were able to mount a successful axon regeneration relying on other mechanisms (**Fig. 6m**).

Binding motifs for bHLH-PAS TFs are enriched in DhMRs after PL and a link between AhR and Bmal1

TFs often collaborate with chromatin regulators to rewire gene circuits through epigenetic reconfiguration such as DNA hydroxymethylation catalyzed DNA methylcytosine dioxygenase Tet3 [52,53]. Tet3 is upregulated by PL but not CL and is required for the conditioning effect [52]. In our previous genome-wide profiling of differentially hydroxymethylated regions (DhMRs) after DRG axotomy, we had identified 1,036 PL-specific DhMRs at 1 dpi, mostly residing in gene bodies or non-coding regions (**Fig. S17a, b**) [3,53].

Interestingly, our recent study found that PL-DhMRs are enriched for binding motifs of many bHLH-PAS TFs, including Bmal1, Clock, HIF-1α, and Arnt, but not AhR [3]. In fact, the HRE motif was found

in 436 PL-DhMRs (~40%), corresponding to 766 associated genes (**Fig. S17c, Table S16**). We assessed the transcriptional state of these 766 genes by intersecting them with PL-RAGs, revealing 169 common genes featuring Circadian Rhythm (linking HIF and Bmal1) and notably Neurotrophin/Tyrosine kinase receptor pathway (**Fig. S17d, e, Table S17**).

Further overlap analysis revealed that the genes associated with PL-DhMR/HRE shared 19 or 8 common genes with the *Ahr* cKO DEGs in naive or axotomized DRG, receptivity (**Fig. S17f, g**), suggesting that HRE-driven genes as a result of *Ahr* deletion may operate through DhMRs (residing mostly at gene bodies, rather than promoters [3,53]). Additionally, consistent with changes in GADD45 pathway (shown in **Fig. S14b**), which is linked to DNA demethylation, we found that *Ahr* deletion also led to increased global level of 5hmC in axotomized DRG neurons at 2 dpi, thus further linking AhR, HIF and Bmal1 (**Fig. S17h, i**).

Since Bmal1 gates regenerative responses of DRG neurons partly through Tet3/5hmC gain [3], we thus compared the Bmal1 and AhR axotomy-associated regulons, which revealed a large repertoire of unique genes as well as 21 common genes, featuring neuronal pathways, PPAR signaling, steroid hormone biosynthesis, and drug metabolism, etc. (**Fig. S18a, Table S18**). Hence, Bmal1 and AhR, and for that matter, HIF-1α, seem to take up different transcriptional tasks in preparing DRG for axonal injury.

Another link between circadian and AhR was indicated by the finding that xenobiotic metabolism/AHR signaling were top enriched pathways of the *Bmal1* cKO regulon [3] upon PL (**Fig. S18b, c**). This implicated Bmal1 circadian as a potential upstream regulator of AhR signaling. In this context, it is notable that *Cyp1b1* exhibited diurnal transcriptional changes in DRG (**Fig. S18d**).

AhR antagonist induces RAGs and regulators of RNA Polymerase III and ISR after axotomy

So far, we showed that *Ahr* cKO was able to rewire gene regulatory circuits in both naive and axotomized

DRG, corresponding to enhanced axon growth. To evaluate translational relevance, we tested pharmacological manipulation of AhR activity after axotomy by delivering AhR agonist ITE or antagonist TMF at 1 hr after PL, followed by two additional injections at 1 and 2 dpi, and analysis of DRG at 3 dpi (**Fig. 7a**). Results showed that AhR antagonist augmented PL-triggered induction of well-known RAGs, including *Bdnf, Atf3, Sprr1a, Gal,* and *Npy,* while AhR agonist exerted no overt effect (**Fig. 7b**). These results support a repressive role of AhR for RAGs induction, which can be alleviated by pharmacological targeting of AhR after PL.

We next leveraged recent scRNA-seq data to further define the neuron-specific AhR regulon in response to PL [54], revealing 98 genes associated with AhR (**Fig. 7c**). Notably, pooled scRNA-seq results from 6 h, 1, 2, 7, 14 dpi predicted inactivation of AhR after PL (in agreement with our model of a transient activation of AhR signaling), in contrast to the activation of well-known regeneration-associated TFs such as ATF3, Sox11, Smad1, Creb1, Myc, Jun, as well as ERG (Egr1, Fos) (**Fig. S19a**). Pathway analysis highlighted enrichment for RNA Polymerases (Pol) regulation (e.g., RNA Pol III transcriptional termination, regulation of transcription by RNA Pol II, Negative regulation of pri-miRNA RNA Pol II) (**Fig. 7d**).

RNA Pol III transcribes small RNA including transfer (t)RNA and S5 ribosomal (r)RNA [55], potentially impacting global protein translation. We next assessed the impact of in vivo pharmacological manipulation of AhR on *Nfia* and *Nfib,* two genes involved in transcriptional termination of RNA Pol III and both containing AHRE in promoter. We found that AhR antagonist TMF resulted in suppression of *Nfia* and *Nfib*, whereas agonist ITE exerted no effect (**Fig. 7e, S19b**). We also analyzed genes of the GO terms that were enriched in the 98 DRG neuron-specific AhR-regulated genes. We found *Sox9* and *Rest* (GO term of Negative regulation of Neural differentiation) and *Cdk6* (GO term of Gliogenesis), all containing AHRE and HRE in promoter, as well as *Stmn* (encoding SCG10, a widely used marker of

sensory axon regeneration), showed upregulation by TMF but were not affected by ITE upon PL (**Fig. 7e, S19b**).

Finally, analysis of scRNA-seq data of axotomized DRG [54] also showed activation of a number of TFs acting as sensors in ISR, e.g.,ATF4, ATF6, and Ddit3 [56] (**Fig. S19a)**. Intriguingly, *Atf4*, a TF activated by increased cellular levels of uncharged tRNA [57], harbors AHRE in promoter and it was induced early after PL in majority of DRG neurons subtypes, and displayed inverse activation state relative to AhR (**Fig. S19a, c, d**). Further assessment of the impact of AhR inhibition by TMF on these ISR regulators revealed a general downregulation (**Fig. 7f**), signifying that AhR inhibition partly operates through repression of ISR.

Discussion

Injured neurons need to respond to environmental stressors while balancing regenerative needs. Here, we uncovered a role of AhR in engaging tissue-protective gene networks for xenobiotic metabolism, inflammation, and ISR, but at the expense of axon regeneration. AhR inhibition can shift the balance towards regenerative gene programs to accelerate axon regeneration (**Fig. 7g**).

All organisms are continuously exposed to external chemicals, known as xenobiotics, and xenobiotic detoxification systems emerged early in evolution as a protective mechanism, mainly through drug-metabolizing enzymes and transporters to mitigate toxicity. AhR is well known for its involvement in toxicology and carcinogenesis; its neuronal functions are less well-defined, even though AhR is widely expressed in the nervous system (in invertebrates almost exclusively in neurons) [58,59]. The detoxification function of AhR may be a late evolutionary adaptation, pointing to a central role of AhR in neural homeostasis, synaptic function, and cell fate specification [58]. Genetic disruption of *Ahr* homologs in *C. elegans* or in *Drosophila* affected axon and dendritic branching [59,60]. Similarly, *Ahr* deletion in mouse led to increased dendrite branching and spine density of hippocampal neurons, affecting learning and memory [61], while *Ahr* cKO in cerebellar granule neuron precursors promoted differentiation and neurite outgrowth [62]. Our current study thus extends the neuronal functions of AhR as key regulator of axonal injury response. In echo, an unbiased high throughput screen combined with analysis of TF binding sites computationally predicted AhR as a regulator of axon growth [63] .

Axon regeneration requires concerted transcriptional regulation to induce RAGs. Previously, we and others have identified a set of regeneration-associated TFs [20,44,64,65] and epigenetic regulators [53,66,67] after conditioning lesion of DRG. However, the functional diversity of the regeneration-associated TFs, their collaboration or antagonism, downstream targets, or links to epigenetics remain opaque. Here, we

showed responsiveness of DRG neurons to ligand-mediated AhR signaling, evidenced by cytoplasm-nuclear shuttling of AhR and transcriptional changes of canonical detox target genes (*Cyp1a1* and *Cyp1b1*). Peripheral nerve lesion resulted in early induction of AhR and HIF-1α, fitting with enrichment of both xenobiotic metabolism and hypoxia gene sets in DRG transcriptomes at 1 dpi. As a transcription factor, AhR controls a large repertoire of target genes via AHRE and second-wave downstream genes involved in a wide range of biological processes. AhR activation appeared to be transient despite prolonged elevation of protein levels, consistent with multiple negative feedback mechanisms including induction of Cyp1 enzymes to degrade AhR ligands, upregulation of AhRR to compete for Arnt and AHRE occupancy, downregulating Kyat1 to limit production of local AhR ligands, and induction of HIF-1α . In addition, ligand-activated AhR is also subject to ubiquitination and proteasomal degradation [6]. The transient nature of AhR activation is not only important to prevent detrimental overactivity effects; but also releases Arnt for HIF signaling, thus another aspect to consider is that the promoting effect of intermittent hypoxia [4] may operate through AhR inhibition.

While functional assays suggested that the growth advantage of *Ahr*^{cKO} DRG neurons required HIF-1α, the signaling relationship between the two pathways appears complex, reflected by overall collaboration (as *Ahr* cKO led to suppression of Hypoxia gene set), but antagonism on individual gene level. In this context, it is worth discussing that HRE-driven genes as a result of *Ahr* cKO (e.g. neurotrophin pathway genes) may operate through PL-DhMR/HRE (residing in gene bodies), independent of Hypoxia signature genes driven by HRE in promoter. Apart from Arnt, other proteins may also be involved in AhR and HIF signaling [14,68]. For instance, AhR is implicated in the transcriptional regulation of non-AHRE containing genes through interaction with other TFs [68-70], epigenetic regulators [71-73] , as well as acting as an E3 ubiquitin-ligase controlling the stability and thereby potency of its associated TFs [74].

Our comparative transcriptomics unveiled the molecular underpinning of the growth promoting

phenotype of *Ahr* deletion, highlighting suppression of acute stress and inflammation, in line with the well-documented function of AhR as an environmental sensor for dietary metabolites/pollutants or injury metabolites to upregulate detoxification enzymes to maintain homeostasis, as well as a sensor of ROS and mediator of oxidative stress response [6]. *Ahr* cKO mimicked the conditioning lesion in launching axonogenesis gene programs, consistent with accelerated axon regeneration after PL at early timepoints of 1 to 3 dpi. Interestingly, the DEGs did not include well-known RAGs such as *Atf3*, *Npy*, *Gap43*, but instead involved new pathways such as Phagosome formation and carbohydrate metabolism, while neuronal specific AhR-dependent genes further included regulation of RNA polymerase III, as well as ISR.

Our data also revealed the interconnectedness of bHLH-PAS TFs in regulating axonal injury and regenerative responses, linking circadian regulation (Bmal1) [3], hypoxia response (HIF), and xenobiotic metabolism (AhR), each controlling distinct but also shared target genes. Bmal1 appeared to be an upstream regulator of AhR/xenobiotic pathways, with *Cyp1b* displaying diurnal transcriptional changes. while HIF also controls circadian pathways. Our studies also identified enrichment of binding motifs of these bHLH-PAS TFs in DNA hydroxymethylation regions upon PL. In this context, it is worth mentioning that exposure to AhR ligands often led to methylation changes around AHRE [75]; in echo, GADD45 is featured in AhR cKO transcriptomic changes, and we observed a global 5hmC gain in axotomized DRG neurons. Hence, AhR may contribute to gene changes by modulating DNA (hydroxy)methylation.

From a therapeutic point of view, we demonstrated that in vivo administration of AhR antagonist at 1 hr after the onset of axotomy induced RAGs such as *Bdnf, Atf3, Sprr1a, Gal1* and *Npy* (unlike in non-injury setting or *Ahr* genetic ablation). Hence, the effect of AhR antagonist on gene expression is influenced by the duration of AhR inhibition, temporal relationship to axonal injury, and the abundance or potency

of endogenous AhR ligands. The sources and identity of AhR endobiotic (endogenous compounds) or xenobiotic ligands (a.k.a xenokines) or proligands will be difficult to identify, as injury metabolites may arise locally inside axotomized DRGs or originate via circulation from systemic inflammation. Future studies are needed to test the efficacy of AhR antagonist delivered at a particular time window and optimal dosage to accelerate nerve repair. In this context, weak AhR agonist may function as AhR antagonist in the presence of potent endogenous ligands. AhR plays a prominent role in safe-guarding the protective function of barrier tissues including skin, lung, and guts, as well as immunity [76]. Intriguingly, the gut-metabolite indole-3-propionate (IPA), produced by intermittent fasting, promotes axon regeneration through immune-mediated mechanism [77], but the link to neuronal AhR activation is unclear. Ahr can also be activated by oxidative stress, independent of ligands [78].

Echoing our findings, inhibition AhR also has also been shown to be beneficial for CNS diseases such as stroke, wherein *Ahr* deletion or antagonist administration led to reduced infarct volume and gliosis, along with improved motorsensory recovery [79]. In a Huntington's disease model, *Ahr* deletion led to protection against neurotoxicity and oxidative stress [80]. Recent studies also reported the role of endothelial AhR signaling in integrating dietary cues to maintain tissue homeostasis [81] and exerting protective function in the gut-lung axis [82]. AhR is also important for timely termination of the regenerative response of intestinal epithelia by restricting chromatin accessibility of regeneration-associated Yap/Tead target genes in colonic stem cells [83]. There also exists naturally occurring AhR polymorphism within and across species, leading to significant differences in the sensitivity and response to AhR ligands [6]; whether that might lead to different axon regenerative capacity, and whether different dietary regimens or unique pathogen loads would be a factor awaits future studies. Also notable is that constitutive expression of *Cyp1a1* gene partially phenocopies *Ahr* null phenotype by reducing cognate ligand of AhR [9], thus offering an alternative way to modulate AhR activity.

In summary, our studies provide new understanding of an antagonizing role of AhR for axon regeneration. Our results on the crosstalk of AhR with HIF and epigenetic mechanisms will help advancing new strategies to enhance axon regeneration and nerve repair.

Methods

Animals

All animal studies were performed under protocols approved by the Institutional Animal Care and Use Committee (IACUC) of Icahn School of Medicine at Mount Sinai. Animals were housed in a pathogen-free barrier facility, under a 12-hour light:dark cycle with food and water provided *ad libitum*.

C57BL/6J mice (JAX stock no. 000664), *Ahr*$^{fl/fl}$ mice (*Ahr*$^{tm3.1Bra}$/J; stock no. 006203), Nestin-Cre mice (B6.Cg-Tg(Nes-cre)1Kln/J; stock no. 003771), Thy1-CreER^{T2} mice (Tg(Thy1-cre/ERT2,-EYFP)HGfng/PyngJ; stock no. 012708), and Rosa26^{INTACT} mice (B6;129-Gt(ROSA)26Sor$^{tm5(CAG-Sun1/sfGFP)Nat}$/J; stock no. 021039) were obtained from Jackson Laboratory. *Arnt*$^{fl/fl}$ mice were obtained from Frank Gonzalez, NIH. All mice were bred on a C57BL/6J genetic background. Littermates were used as control groups. To induce deletion of the target genes, tamoxifen (Sigma T5648), dissolved in corn oil (Sigma C8267), was injected intraperitoneally at a dose of 100 mg/kg daily for 5 days.

The following primers were used for genotyping by PCR using mouse tail DNA:

Ahr$^{fl/fl}$ mice: F1: GTCACTCAGCATTACACTTTCTA, F2: CAGTGGGAATAAGGCAAGAGTGA, R1: GGTACAAGTGCACATGCCTGC. Expected band sizes: 106 bp for wildtype allele, 140 bp for floxed allele, and 180 bp for excised floxed allele.

Arnt$^{fl/fl}$ mice: F1: TGCCAACATGTGCCACCATGT, R1: GTGAGGCAGATTTCTTCCATGCTC. 290 bp for wild type allele, 340 bp for Arnt floxed allele.

Nestin-Cre mice: F1: CCGCTTCCGCTGGGTCACTGT, R1: TGAGCAGCTGGTTCTGCTCCT, R2: ACCGGCAAACGGACAGAAGCA. 379 bp for wild type allele, 229 bp for transgenic Cre allele.

Rosa26^{INTACT} mice: F1: GCACTTGCTCTCCCAAAGTC, R1: CATAGTCTAACTCGCGACACTG, R2: GTTATGTAACGCGGAACTCC. 557 bp for wild type allele, 300 bp for knockin allele.

Thy1-CreER^{T2} mice: F1: TCTGAGTGGCAAAGGACCTTAGG, R1: CGCTGAACTTGTGGCCGTTTACG, Int-F2: CAAATGTTGCTTGTCTGGTG, Int-R2: GTCAGTCGAGTGCACAGTTT. 200 bp for wild type allele, 300 bp for transgenic Cre allele.

Sciatic nerve lesion

Male and female mice, age 8-10 weeks old, were anesthetized by isofluorane inhalation (5% for induction, 2% for maintenance). A small skin incision was made at mid-thigh using a scalpel blade after skin preparation and disinfection. To clearly expose the sciatic nerve, the fascial space between biceps femoris and gluteus superficialis muscles was opened gently without hemorrhage. The nerve was then freed from surrounding connective tissue under microscope, avoiding shearing or traction force. For sciatic nerve crush model, the nerve was crushed with an Ultra-fine Hemostat (Fine Science Tools #13020-12) for 15 sec at the third click. For sciatic nerve transection model, the nerve was cut with a 3 mm Vannas Spring Scissor (Fine Science Tools #15000-00). For sham surgery, the contralateral sciatic nerve was exposed as described but left intact. Mouse skin was closed with Reflex 7 mm Wound Closure System (Braintree Scientific RF7 CS) after surgery. Mice were left to recover in a warm cage. All surgical instruments were autoclaved before surgery and principles of asepsis were maintained throughout.

DRG neuron culture and neurite outgrowth assay

Adult DRG from adult C57BL/6J mice (8-10 weeks old) were rapidly dissected and placed in ice-cold DMEM/F12 (Gibco 11330057). DRG were washed 3 times with ice-cold calcium- and magnesium-free HBSS (Gibco 14175095) including 10 mM HEPES (Gibco 15630106) before incubating in 0.3% collagenase I (Worthington LS004196) for 90 min at 37°C. DRG were then washed 3 times with HBSS buffer with HEPES at room temperature, followed by additional digestion in 0.25% trypsin-EDTA (Gibco 25200072) containing 50 µg/ml DNase I (Worthington LK003172) for 30 min at 37°C. Trypsinization was stopped with warm DMEM medium (Gibco 10569044) containing 10% FBS (Gibco 26140079) and DNase I. DRG were dissociated by trituration with fire-polished Pasteur glass pipets

(Fisherbrand 13-678-20D). To remove myelin debris and cell clumps, a partial-purification step was performed by centrifugation through a BSA (Fisher BioReagents BP9700100) cushion. Specifically, the DRG suspension was mixed with 8 ml NS-A Basal Medium (NeuroCult 05750) and then 2 ml of 15% BSA in HBSS was added at the bottom of the 15 ml centrifuge tube followed by centrifugation at 1,000 rpm for 6 min. Supernatant was carefully removed and DRG were resuspended in NS-A Basal medium containing 2% B27 (Gibco A3582801), 0.725% Glucose, 0.5mM L-Glutamine, and 0.4% Antibiotic-Antimycotic (Gibco, 15240062). DRG neurons were plated on Poly-L-ornithine (Sigma P4957) and laminin (Gibco 23017015) coated chamber slides or 6-well plates for subsequent experiments.

For neurite outgrowth assay, L4-L6 DRG neurons from mice of different genotypes were prepared as described above and seeded on pre-coated 4-well chambered slides (Falcon 10384501), at approximately 1,000-2,000 neurons per well. Neurons were fixed with ice-cold 4% PFA and stained with anti-Tubulin β3 (clone TUJ1, Biolegend 801201, 1:1,000) to visualize regenerating neurites. The length of the longest neurite of each neurite-bearing neuron (neurite longer than the diameter of its soma) was measured using the ImageJ plugin simple neurite tracer (SNT, version 4.0.3) [84].

For pharmacological experiments, DRG from wild-type C57BL/6J mice were prepared as described above and plated on pre-coated 6-well plate, using neurons from 8-10 DRG per well. Neurons were cultured for 24 hr with endogenous AhR agonists ITE (25 μM, Tocris 1803), L-Kynurenine (25 μM, Tocris 4393), or antagonist CH 223191 (25 μM, Tocris 3858). All drugs were dissolved in DMSO. Cells were lysed for RNA extraction or fixed for immunofluorescence staining.

qRT-PCR

Total RNA of cells or tissues was extracted with the RNeasy Plus Micro kit (QIAGEN 74034) or RNeasy Plus Mini kit (QIAGEN 74134), respectively. For RNA collection from tissue, dissected DRGs were

initially stored in RNAlater Stabilization Solution (Invitrogen AM7024), and then homogenized in RLT Plus buffer including 1% β-mercaptoehanol using RNase-free disposable pellet pestles (Fisherbrand 12-141-364). For RNA collection from cells, cell cultures were washed once with PBS and then lysed by vigorous pipetting. Genomic DNA was eliminated through a gDNA eliminator column according to the manufacturer's instructions. RNA was eluted in RNase-free water and stored at -80°C. cDNA was prepared with the SuperScript III First-Strand Synthesis System (Invitrogen 18080051) from equal amounts of RNA (approximately 200 ng from DRG tissues and 500 ng from cell culture for each reaction). The quantitative RT-PCR (qRT-PCR) was performed with PerfeCTa SYBR Green FastMix Rox (Quanta Bioscience 95073-012) with an ABI 7900HT quantitative PCR system (Applied Biosystems) at the Mount Sinai qPCR CoRE. *Hprt* was used as the house-keeping gene to normalize qRT-PCR results. The qRT-primers are listed in supplemental **Table S19**.

Western blot

L4-L6 DRG were collected and immediately frozen in liquid nitrogen and stored at -80°C for later analysis. Tissues were homogenized and lysed with RIPA buffer (Sigma R0278) containing EDTA-free protease inhibitor cocktail (Roche 04693159001) and phosSTOP (Roche 4906845001). The frozen DRG in a 1.5 ml tube were disrupted with RNase-free disposable pellet pestles (Fisherbrand 12-141-364) on ice. 1 U/μl benzonase nuclease (Millipore E1014) was added to lysis buffer. Samples were mixed on a rotator at 4°C for 30 min and then spun in a table top centrifuge at 13,000 rpm for 10 min to remove tissue pellet. An equal volume of 4x LDS sample buffer (Invitrogen NP0008) was added to lysates, which were then boiled at 95°C for 5 min. Lysate from equal number of DRGs was loaded and separated by electrophoresis on 4-12% ExpressPlus gels (Genscript M41210), followed by transfer to a PVDF membrane. Membranes were blocked in Intercept Blocking Buffer (LI-COR Biosciences 927-70001) at room temperature for 1 hr and subsequently incubated with primary antibodies diluted with Intercept Antibody Diluent (LI-COR Biosciences 927-75001) at 4°C overnight. Blots were washed with PBST (5

x 5 min) and incubated with secondary antibodies at room temperature for 1 hr. Bands were detected with the Odyssey Infrared Imaging System (LI-COR Biosciences) and band intensity was quantified with Image Studio 5.2.5 (LI-COR Biosciences).

The following primary antibodies were used for WB:

anti-AHR (rabbit, used as 1:1,000 dilution, Enzo BML-SA210),

anti-CYP1B1 (rabbit, 1:1,000, Invitrogen PA5-95277),

anti-HIF1α (rabbit, 1:500, Novus NB100-479),

anti-ATF3 (rabbit, 1:1,000, Santa Cruz sc-188),

anti-β-Actin (mouse, 1:10,000, Sigma A1978).

The following secondary antibodies and their dilutions were used for WB:

800CW donkey anti-rabbit IgG (1:10,000, LI-COR Biosciences 926-32213),

680RD donkey anti-mouse IgG (1:10,000, LI-COR Biosciences 926-68072).

Immunofluorescence

For immunofluorescence (IF) of cultured cells, cultures were washed once with PBS and then fixed in 4% ice-cold PFA for 15 min. For IF of cryosections of DRG and sciatic nerves, tissues were fixed in 4% ice-cold PFA/PBS for 12 hr, washed in PBS, and then embedded in OCT compound (Fisher Scientific 23-730-571). Cryosections were cut at 12 µm thickness and placed on SuperFrost Plus slides (VWR 48311-703) and stored at -20°C before analysis. Sections were washed with PBS and incubated in blocking buffer containing 5% normal donkey serum (Jackson Immunoresearch 017-000-121) and 0.3% Triton X-100 (Acros Organics 9002-93-1) in PBS for 1 hr at room temperature. Primary antibodies (details below) were diluted in antibody dilution buffer containing 1% BSA (Fisher BioReagents BP9700100) and 0.3% Triton X-100 in PBS and incubated at 4°C overnight. Alexa-coupled secondary antibodies were diluted in antibody dilution buffer and added on sections after 3x washing with PBS and

incubated for 1 hr at room temperature. DAPI (Invitrogen D1306) was used for nuclear counterstaining (1:1,000). Slides were washed 3x with PBS and mounted with Fluromount G (Southern Biotech 0100-01). IF images were captured using a Zeiss microscope with AxioCam MRm camera.

The following primary antibodies were used for IF:

anti-AHR (rabbit, 1:300, Enzo BML-SA210),

anti-ATF3 (rabbit, 1:300, Santa Cruz sc-188),

anti-Tubulin β3 (TUBB3, clone TUJ1, mouse, 1:1,000, Biolegend 801201),

anti-Tubulin β3 (TUBB3, clone TUJ1, rabbit, 1:300, Cell Signaling 5568S),

anti-SCG10/STMN2 (rabbit, 1:1,000, Novus NBP1-49461),

anti-GFP (chicken, 1:1,000, Aves Lab GFP-1020),

anti-IBA1 (rabbit, 1:1,000, Wako 019-19741),

anti-pSMAD1/5/8(rabbit, 1:1,000, Cell Signaling 9511),

anti-GAP43(rabbit, 1:1,000, Sigma AB5220),

anti-pCREB (rabbit, 1:300, Cell Signaling 9198),

anti-pS6KS235/236 (rabbit, 1:300, Cell Signaling 2211),

anti-CD45(rat, 1:50, BD Bioscience 550539),

anti-5hmC (rabbit, 1:500, Active Motif 39769).

The following Alexa-conjugated donkey secondary antibodies (Jackson ImmunoResearch) were used at 1:300 dilution of a 1 mg/ml stock solution (in 50% glycerol).

AlexaFluor 488 anti-rabbit IgG (711-545-152),

AlexaFluor 488 anti-chicken IgY (703-545-155),

AlexaFluor 594 anti-rabbit IgG (711-585-152),

AlexaFluor 594 anti-mouse IgG (711-585-150),

AlexaFluor 594 anti-rat IgG (712-585-153),

AlexaFluor 647 anti-rabbit IgG (711-605-152),

AlexaFluor 647 anti-mouse IgG (715-605-151).

Measurement of in vivo sciatic nerve regeneration index.

Sciatic nerves from animals with crush injury were collected at 1 to 3 days post injury. Cryosections were prepared as described above and stained with anti-SCG10 antibody. Tiled images of sciatic nerves were merged using Photoshop CC 2019. The SCG10 fluorescence intensity was measured along the length of the nerve using ImageJ (version 2.3.0/1.53q). A rectangular region-of-interest (ROI) containing the lesion site and adjacent proximal and distal areas was selected to generate a 'plot profile'. The 'plot profile' function displays column-average gray values, with x-axis representing horizontal distance and y-axis averaged pixel intensity of columns. The position with maximal SCG10 profile intensity was used to normalize the regeneration index and the position with minimal intensity was used for subtraction of background value.

Motor and sensory behavioral testing

All behavioral tests were performed at the beginning of the mouse active phase (after 7 pm; mice were kept at 7 am – 7 pm light cycle) by an investigator who was blinded to the cohort identities.

All animals were acclimated to the isolated procedure room for 30 min before testing. For motor function recovery testing, paw prints of different groups were collected from control mice or mice that had undergone sciatic nerve injury. Hind paws of mice were pressed on an ink pad and mice were then allowed to walk on white paper to collect the prints. The Sciatic Functional Index (SFI) was calculated to measuring dimensions of the paw prints [85]. The SFI was calculated with the following formula:

SFI = -38.3×(EPL-NPL)/NPL + 109.5×(ETS-NTS)/NTS + 13.3×(EIT-NIT)/NIT - 8.8

(E-, Experimental-; N-, Normal-; PL, Print Length; TS, Total Spread; IT Intermediate Toes).

For testing of sensory function recovery, von Frey filament tests were performed [86]. Briefly, the plantar

surface of the hind paw was pricked with a series of fine filaments and the mechanical threshold that evoked a withdrawal reflex was recorded.

RNA-seq analysis

For next-generation sequencing, RNA was isolated from DRG tissue with the QIAGEN RNeasy plus mini kit sequenced on the Illumina NovaSeq platform (Psomagen, Inc). Preprocessing, quality control, and alignment of FASTQ files was performed using the NGS-Data-Charmer pipeline. Trim-Galore tool (v0.6.5) [87] was used for adaptor trimming and aligned to the mouse mm10 genome assembly using Bowtie2 (v2.4.1) [88]. The 'rmdup' module of SAMtools (v1.10) [89] was used to remove duplicated read pairs. FeatureCounts was used to obtain a gene expression matrix, using the parameters "--fraction -t gene" on the GENCODE annotation (vM25). Genes with fewer than 5 samples showing a minimum read count of 2 reads were filtered out before performing differentiation gene expression analysis with DESeq2.

Bioinformatics

TF interaction networks were generated using STRING database [26], using the default setting of medium confidence. Targeted TF binding motif analysis RAGs was identified using Homer package [90]. ChIP-X Enrichment Analysis was performed using ChEA3 [45]. Heatmaps and volcano plots were generated with FLASKi [91] and OriginLab respectively. Volcano plot Gene set enrichment analysis (GSEA) was performed using GSEA_4.3.2 software provided by the Broad Institute [92], using the non-pre ranked whole DRG genome and Hallmark_MSigDB gene sets. Pathway enrichment in gene sets was identified using performed with IPA Qiagen knowledge database [93] and Enrichr [94,95], as indicated. IPA was also used to generate graphical summary and identify upstream regulators using default settings. Identification of experimentally validated promoter motifs was conducted using the Eukaryotic Promoter Database platform [96].

Statistical analysis

For each dataset, Shapiro-Wilk test was performed to test data normality ($P > 0.05$ determined as parametric and $P < 0.05$ determined as nonparametric). For parametric data, unpaired two-tailed Student's *t*-test was used for comparison between two groups, one-way analysis of variance (ANOVA) with Holm-Sidak multiple test correction was performed for comparison of three groups, and Two-way ANOVA followed by Benferroni's multiple comparisons test was used for multiple groups For nonparametric data, Mann-Whitney two-tailed *t*-test was used for comparison between two groups and Kruskal-Wallis test with Dunn's multiple test correction was performed for comparison between multiple groups. All statistical analyses were performed with GraphPad Prism 9. The mean values are presented in graphs along with the standard error of the mean (SEM) as error bars. Differences were considered as significant with *P*-values of < 0.05 and the asterisks are used to denote significance ($*P < 0.05$, $**P < 0.01$, and $***P < 0.001$).

Data Availability

Source data are provided with this paper. The RNA-seq data of *Bmal1* cKO DRG neurons [3] has been deposited at the NCBI GEO database under accession number GSE233367. The DRG 5hmC sequencing dataset [53] is available under accession code GSE85972.

Acknowledgements

We thank all members from the Zou laboratory for help and suggestions.

This work was supported by funds to H.Z. from NIH (R01 NS127442), the New York State Spinal Cord Injury Research Board (DOH01-C33268GG, DOH01-C30832GG, and DOH01-C32242GG), and Neilsen Foundation (#890112). Y.W. was partly supported by scholarship fund from Xi'an Jiaotong University.

Author contributions

Conceptualization: YW, DH, RHF, HZ; Data acquisition: YW, DH; Data analysis: YW, DH , RHF, HZ; Bioinformatic analysis: ME, DH, YW, AR, LS; Manuscript writing: YW, DH, RHF, HZ.

Competing Interests Statement: All authors declare no competing interests.

References

1 Bersten, D. C., Sullivan, A. E., Peet, D. J. & Whitelaw, M. L. bHLH-PAS proteins in cancer. *Nat Rev Cancer* **13**, 827-841 (2013). https://doi.org/10.1038/nrc3621

2 Mulero-Navarro, S. & Fernandez-Salguero, P. M. New Trends in Aryl Hydrocarbon Receptor Biology. *Front Cell Dev Biol* **4**, 45 (2016). https://doi.org/10.3389/fcell.2016.00045

3 Halawani, D. *et al.* Circadian clock regulator Bmal1 gates axon regeneration via Tet3 epigenetics in mouse sensory neurons. *Nat Commun* **14**, 5165 (2023). https://doi.org/10.1038/s41467-023-40816-7

4 Cho, Y. *et al.* Activating Injury-Responsive Genes with Hypoxia Enhances Axon Regeneration through Neuronal HIF-1alpha. *Neuron* **88**, 720-734 (2015). https://doi.org/10.1016/j.neuron.2015.09.050

5 Rothhammer, V. & Quintana, F. J. The aryl hydrocarbon receptor: an environmental sensor integrating immune responses in health and disease. *Nat Rev Immunol* **19**, 184-197 (2019). https://doi.org/10.1038/s41577-019-0125-8

6 Avilla, M. N., Malecki, K. M. C., Hahn, M. E., Wilson, R. H. & Bradfield, C. A. The Ah Receptor: Adaptive Metabolism, Ligand Diversity, and the Xenokine Model. *Chem Res Toxicol* **33**, 860-879 (2020). https://doi.org/10.1021/acs.chemrestox.9b00476

7 Miao, W., Hu, L., Scrivens, P. J. & Batist, G. Transcriptional regulation of NF-E2 p45-related factor (NRF2) expression by the aryl hydrocarbon receptor-xenobiotic response element signaling pathway: direct cross-talk between phase I and II drug-metabolizing enzymes. *J Biol Chem* **280**, 20340-20348 (2005). https://doi.org/10.1074/jbc.M412081200

8 Tsuji, G. *et al.* Identification of ketoconazole as an AhR-Nrf2 activator in cultured human keratinocytes: the basis of its anti-inflammatory effect. *J Invest Dermatol* **132**, 59-68 (2012). https://doi.org/10.1038/jid.2011.194

9 Schiering, C. *et al.* Feedback control of AHR signalling regulates intestinal immunity. *Nature* **542**, 242-245 (2017). https://doi.org/10.1038/nature21080

10 Vogel, C. F. A. & Haarmann-Stemmann, T. The aryl hydrocarbon receptor repressor - More than a simple feedback inhibitor of AhR signaling: Clues for its role in inflammation and cancer. *Curr Opin Toxicol* **2**, 109-119 (2017). https://doi.org/10.1016/j.cotox.2017.02.004

11 Oshima, M., Mimura, J., Yamamoto, M. & Fujii-Kuriyama, Y. Molecular mechanism of transcriptional repression of AhR repressor involving ANKRA2, HDAC4, and HDAC5. *Biochem Biophys Res Commun* **364**, 276-282 (2007). https://doi.org/10.1016/j.bbrc.2007.09.131

12 Semenza, G. L. Hypoxia-inducible factors in physiology and medicine. *Cell* **148**, 399-408 (2012). https://doi.org/10.1016/j.cell.2012.01.021

13 Vorrink, S. U. & Domann, F. E. Regulatory crosstalk and interference between the xenobiotic and hypoxia sensing pathways at the AhR-ARNT-HIF1α signaling node. *Chem Biol Interact* **218**, 82-88 (2014). https://doi.org/10.1016/j.cbi.2014.05.001

14 Gradin, K. *et al.* Functional interference between hypoxia and dioxin signal transduction pathways: competition for recruitment of the Arnt transcription factor. *Mol Cell Biol* **16**, 5221-5231 (1996). https://doi.org/10.1128/MCB.16.10.5221

15 Mandl, M. & Depping, R. Hypoxia-inducible aryl hydrocarbon receptor nuclear translocator (ARNT) (HIF-1β): is it a rare exception? *Mol Med* **20**, 215-220 (2014). https://doi.org/10.2119/molmed.2014.00032

16 Mascanfroni, I. D. *et al.* Metabolic control of type 1 regulatory T cell differentiation by AHR and HIF1-α. *Nat Med* **21**, 638-646 (2015). https://doi.org/10.1038/nm.3868

17 Gabriely, G., Wheeler, M. A., Takenaka, M. C. & Quintana, F. J. Role of AHR and HIF-1α in Glioblastoma Metabolism. *Trends Endocrinol Metab* **28**, 428-436 (2017). https://doi.org/10.1016/j.tem.2017.02.009

18 Richardson, P. M. & Issa, V. M. Peripheral injury enhances central regeneration of primary sensory neurones. *Nature* **309**, 791-793 (1984). https://doi.org/10.1038/309791a0

19 Neumann, S. & Woolf, C. J. Regeneration of dorsal column fibers into and beyond the lesion site following adult spinal cord injury. *Neuron* **23**, 83-91 (1999). https://doi.org/10.1016/s0896-6273(00)80755-2

20 Zou, H., Ho, C., Wong, K. & Tessier-Lavigne, M. Axotomy-induced Smad1 activation promotes axonal growth in adult sensory neurons. *J Neurosci* **29**, 7116-7123 (2009). https://doi.org/10.1523/jneurosci.5397-08.2009

21 Seijffers, R., Mills, C. D. & Woolf, C. J. ATF3 increases the intrinsic growth state of DRG neurons to enhance peripheral nerve regeneration. *J Neurosci* **27**, 7911-7920 (2007). https://doi.org/10.1523/JNEUROSCI.5313-06.2007

22 Norsworthy, M. W. *et al.* Sox11 Expression Promotes Regeneration of Some Retinal Ganglion Cell Types but Kills Others. *Neuron* **94**, 1112-1120.e1114 (2017). https://doi.org/10.1016/j.neuron.2017.05.035

23 Ruff, C. A. *et al.* Neuronal c-Jun is required for successful axonal regeneration, but the effects of phosphorylation of its N-terminus are moderate. *J Neurochem* **121**, 607-618 (2012). https://doi.org/10.1111/j.1471-4159.2012.07706.x

24 Parikh, P. *et al.* Regeneration of axons in injured spinal cord by activation of bone morphogenetic protein/Smad1 signaling pathway in adult neurons. *Proceedings of the National Academy of Sciences* **108**, E99-E107 (2011). https://doi.org/10.1073/pnas.1100426108

25 Oñate, M. *et al.* Activation of the unfolded protein response promotes axonal regeneration after peripheral nerve injury. *Sci Rep* **6**, 21709 (2016). https://doi.org/10.1038/srep21709

26 Szklarczyk, D. *et al.* The STRING database in 2021: customizable protein-protein networks, and functional characterization of user-uploaded gene/measurement sets. *Nucleic Acids Res* **49**, D605-D612 (2021). https://doi.org/10.1093/nar/gkaa1074

27 Michaelevski, I. *et al.* Signaling to transcription networks in the neuronal retrograde injury response. *Sci Signal* **3**, ra53 (2010). https://doi.org/10.1126/scisignal.2000952

28 Song, J. *et al.* A ligand for the aryl hydrocarbon receptor isolated from lung. *Proc Natl Acad Sci U S A* **99**, 14694-14699 (2002). https://doi.org/10.1073/pnas.232562899

29 Abron, J. D. *et al.* An endogenous aryl hydrocarbon receptor ligand, ITE, induces regulatory T cells and ameliorates experimental colitis. *Am J Physiol Gastrointest Liver Physiol* **315**, G220-G230 (2018). https://doi.org/10.1152/ajpgi.00413.2017

30 Lehmann, G. M. *et al.* The aryl hydrocarbon receptor ligand ITE inhibits TGFβ1-induced human myofibroblast differentiation. *Am J Pathol* **178**, 1556-1567 (2011). https://doi.org/10.1016/j.ajpath.2010.12.025

31 Zhao, B., Degroot, D. E., Hayashi, A., He, G. & Denison, M. S. CH223191 is a ligand-selective antagonist of the Ah (Dioxin) receptor. *Toxicol Sci* **117**, 393-403 (2010). https://doi.org/10.1093/toxsci/kfq217

32 Zeisel, A. *et al.* Molecular Architecture of the Mouse Nervous System. *Cell* **174**, 999-1014.e1022 (2018). https://doi.org/10.1016/j.cell.2018.06.021

33 Walisser, J. A., Glover, E., Pande, K., Liss, A. L. & Bradfield, C. A. Aryl hydrocarbon receptor-dependent liver development and hepatotoxicity are mediated by different cell types. *Proc Natl Acad Sci U S A* **102**, 17858-17863 (2005). https://doi.org/10.1073/pnas.0504757102

34 Giusti, S. A. *et al.* Behavioral phenotyping of Nestin-Cre mice: implications for genetic mouse models of psychiatric disorders. *J Psychiatr Res* **55**, 87-95 (2014). https://doi.org/10.1016/j.jpsychires.2014.04.002

35 Juricek, L. *et al.* AhR-deficiency as a cause of demyelinating disease and inflammation. *Sci Rep* **7**, 9794 (2017). https://doi.org/10.1038/s41598-017-09621-3

36 Shackleford, G. *et al.* Involvement of Aryl hydrocarbon receptor in myelination and in human nerve sheath tumorigenesis. *Proc Natl Acad Sci U S A* **115**, E1319-E1328 (2018). https://doi.org/10.1073/pnas.1715999115

37 Shin, J. E., Geisler, S. & DiAntonio, A. Dynamic regulation of SCG10 in regenerating axons after injury. *Exp Neurol* **252**, 1-11 (2014). https://doi.org/10.1016/j.expneurol.2013.11.007

38 Heimer-McGinn, V. & Young, P. Efficient inducible Pan-neuronal cre-mediated recombination in SLICK-H transgenic mice. *Genesis* **49**, 942-949 (2011). https://doi.org/10.1002/dvg.20777

39 Young, P. *et al.* Single-neuron labeling with inducible Cre-mediated knockout in transgenic mice. *Nat Neurosci* **11**, 721-728 (2008). https://doi.org/10.1038/nn.2118

40 Mo, A. *et al.* Epigenomic Signatures of Neuronal Diversity in the Mammalian Brain. *Neuron* **86**, 1369-1384 (2015). https://doi.org/10.1016/j.neuron.2015.05.018

41 Renthal, W. *et al.* Transcriptional Reprogramming of Distinct Peripheral Sensory Neuron Subtypes after Axonal Injury. *Neuron* **108**, 128-144 e129 (2020). https://doi.org/10.1016/j.neuron.2020.07.026

42 MacPherson, L. *et al.* Aryl hydrocarbon receptor repressor and TiPARP (ARTD14) use similar, but also distinct mechanisms to repress aryl hydrocarbon receptor signaling. *Int J Mol Sci* **15**, 7939-7957 (2014). https://doi.org/10.3390/ijms15057939

43 Cuartero, M. I. *et al.* L-kynurenine/aryl hydrocarbon receptor pathway mediates brain damage after experimental stroke. *Circulation* **130**, 2040-2051 (2014). https://doi.org/10.1161/CIRCULATIONAHA.114.011394

44 Blesch, A. *et al.* Conditioning lesions before or after spinal cord injury recruit broad genetic mechanisms that sustain axonal regeneration: superiority to camp-mediated effects. *Exp Neurol* **235**, 162-173 (2012). https://doi.org/10.1016/j.expneurol.2011.12.037

45 Keenan, A. B. *et al.* ChEA3: transcription factor enrichment analysis by orthogonal omics integration. *Nucleic Acids Res* **47**, W212-W224 (2019). https://doi.org/10.1093/nar/gkz446

46 Liu, Y. *et al.* Repulsive Wnt signaling inhibits axon regeneration after CNS injury. *J Neurosci* **28**, 8376-8382 (2008). https://doi.org/10.1523/JNEUROSCI.1939-08.2008

47 Zou, Y. Wnt signaling in axon guidance. *Trends Neurosci* **27**, 528-532 (2004). https://doi.org/10.1016/j.tins.2004.06.015

48 Liu, C., Li, S., Liu, T., Borjigin, J. & Lin, J. D. Transcriptional coactivator PGC-1alpha integrates the mammalian clock and energy metabolism. *Nature* **447**, 477-481 (2007). https://doi.org/10.1038/nature05767

49 Liang, H. & Ward, W. F. PGC-1alpha: a key regulator of energy metabolism. *Adv Physiol Educ* **30**, 145-151 (2006). https://doi.org/10.1152/advan.00052.2006

50 LeBleu, V. S. *et al.* PGC-1α mediates mitochondrial biogenesis and oxidative phosphorylation in cancer cells to promote metastasis. *Nat Cell Biol* **16**, 992-1003, 1001-1015 (2014). https://doi.org/10.1038/ncb3039

51 Narita, T. *et al.* Identification of a novel small molecule HIF-1alpha translation inhibitor. *Clin Cancer Res* **15**, 6128-6136 (2009). https://doi.org/10.1158/1078-0432.CCR-08-3180

52 Weng, Y. L. *et al.* An Intrinsic Epigenetic Barrier for Functional Axon Regeneration. *Neuron* **94**, 337-346 e336 (2017). https://doi.org/10.1016/j.neuron.2017.03.034

53 Loh, Y. E. *et al.* Comprehensive mapping of 5-hydroxymethylcytosine epigenetic dynamics in axon regeneration. *Epigenetics* **12**, 77-92 (2017). https://doi.org/10.1080/15592294.2016.1264560

54 Wang, K. *et al.* Single-cell transcriptomic analysis of somatosensory neurons uncovers temporal development of neuropathic pain. *Cell Res* **31**, 904-918 (2021). https://doi.org/10.1038/s41422-021-00479-9

55 Dieci, G., Fiorino, G., Castelnuovo, M., Teichmann, M. & Pagano, A. The expanding RNA polymerase III transcriptome. *Trends Genet* **23**, 614-622 (2007). https://doi.org/10.1016/j.tig.2007.09.001

56 Costa-Mattioli, M. & Walter, P. The integrated stress response: From mechanism to disease. *Science* **368** (2020). https://doi.org/10.1126/science.aat5314

57 Harding, H. P. *et al.* Regulated translation initiation controls stress-induced gene expression in mammalian cells. *Mol Cell* **6**, 1099-1108 (2000). https://doi.org/10.1016/s1097-2765(00)00108-8

58 Huang, X., Powell-Coffman, J. A. & Jin, Y. The AHR-1 aryl hydrocarbon receptor and its co-factor the AHA-1 aryl hydrocarbon receptor nuclear translocator specify GABAergic neuron cell fate in C. elegans. *Development* **131**, 819-828 (2004). https://doi.org/10.1242/dev.00959

59 Qin, H. & Powell-Coffman, J. A. The Caenorhabditis elegans aryl hydrocarbon receptor, AHR-1, regulates neuronal development. *Dev Biol* **270**, 64-75 (2004). https://doi.org/10.1016/j.ydbio.2004.02.004

60 Crews, S. T. & Brenman, J. E. Spineless provides a little backbone for dendritic morphogenesis. *Genes Dev* **20**, 2773-2778 (2006). https://doi.org/10.1101/gad.1487706

61 de la Parra, J. *et al.* AhR Deletion Promotes Aberrant Morphogenesis and Synaptic Activity of Adult-Generated Granule Neurons and Impairs Hippocampus-Dependent Memory. *eNeuro* **5** (2018). https://doi.org/10.1523/ENEURO.0370-17.2018

62 Dever, D. P. *et al.* Aryl hydrocarbon receptor deletion in cerebellar granule neuron precursors impairs neurogenesis. *Dev Neurobiol* **76**, 533-550 (2016). https://doi.org/10.1002/dneu.22330

63 Geeven, G. *et al.* LLM3D: a log-linear modeling-based method to predict functional gene regulatory interactions from genome-wide expression data. *Nucleic Acids Res* **39**, 5313-5327 (2011). https://doi.org/10.1093/nar/gkr139

64 Hervera, A. *et al.* Reactive oxygen species regulate axonal regeneration through the release of exosomal NADPH oxidase 2 complexes into injured axons. *Nat Cell Biol* **20**, 307-319 (2018). https://doi.org/10.1038/s41556-018-0039-x

65 Palmisano, I. *et al.* Epigenomic signatures underpin the axonal regenerative ability of dorsal root ganglia sensory neurons. *Nat Neurosci* **22**, 1913-1924 (2019). https://doi.org/10.1038/s41593-019-0490-4

66 Finelli, M. J., Wong, J. K. & Zou, H. Epigenetic regulation of sensory axon regeneration after spinal cord injury. *J Neurosci* **33**, 19664-19676 (2013). https://doi.org/10.1523/JNEUROSCI.0589-13.2013

67 Wong, J. K. & Zou, H. Reshaping the chromatin landscape after spinal cord injury. *Front Biol (Beijing)* **9**, 356-366 (2014). https://doi.org/10.1007/s11515-014-1329-8

68 Wilson, S. R., Joshi, A. D. & Elferink, C. J. The tumor suppressor Kruppel-like factor 6 is a novel aryl hydrocarbon receptor DNA binding partner. *J Pharmacol Exp Ther* **345**, 419-429 (2013). https://doi.org/10.1124/jpet.113.203786

69 Ohtake, F. *et al.* Modulation of oestrogen receptor signalling by association with the activated dioxin receptor. *Nature* **423**, 545-550 (2003). https://doi.org/10.1038/nature01606

70 Jackson, D. P., Li, H., Mitchell, K. A., Joshi, A. D. & Elferink, C. J. Ah receptor-mediated suppression of liver regeneration through NC-XRE-driven p21Cip1 expression. *Mol Pharmacol* **85**, 533-541 (2014). https://doi.org/10.1124/mol.113.089730

71 Wang, S. & Hankinson, O. Functional involvement of the Brahma/SWI2-related gene 1 protein in cytochrome P4501A1 transcription mediated by the aryl hydrocarbon receptor complex. *J Biol Chem* **277**, 11821-11827 (2002). https://doi.org/10.1074/jbc.M110122200

72 Jin, H. L. & Jeong, K. W. Regulation of aryl hydrocarbon receptor-mediated transcription in human retinal pigmented epithelial cells. *Biochem Biophys Res Commun* **472**, 366-372 (2016). https://doi.org/10.1016/j.bbrc.2016.03.006

73 Joshi, A. D., Hossain, E. & Elferink, C. J. Epigenetic Regulation by Agonist-Specific Aryl Hydrocarbon Receptor Recruitment of Metastasis-Associated Protein 2 Selectively Induces Stanniocalcin 2 Expression. *Mol Pharmacol* **92**, 366-374 (2017). https://doi.org/10.1124/mol.117.108878

74 Ohtake, F. *et al.* Dioxin receptor is a ligand-dependent E3 ubiquitin ligase. *Nature* **446**, 562-566 (2007). https://doi.org/10.1038/nature05683

75 Winans, B. *et al.* Linking the aryl hydrocarbon receptor with altered DNA methylation patterns and developmentally induced aberrant antiviral CD8+ T cell responses. *J Immunol* **194**, 4446-4457 (2015). https://doi.org/10.4049/jimmunol.1402044

76 Stockinger, B., Shah, K. & Wincent, E. AHR in the intestinal microenvironment: safeguarding barrier function. *Nat Rev Gastroenterol Hepatol* **18**, 559-570 (2021). https://doi.org/10.1038/s41575-021-00430-8

77 Serger, E. *et al.* The gut metabolite indole-3 propionate promotes nerve regeneration and repair. *Nature* **607**, 585-592 (2022). https://doi.org/10.1038/s41586-022-04884-x

78 Xiao, W., Son, J., Vorrink, S. U., Domann, F. E. & Goswami, P. C. Ligand-independent activation of aryl hydrocarbon receptor signaling in PCB3-quinone treated HaCaT human keratinocytes. *Toxicol Lett* **233**, 258-266 (2015). https://doi.org/10.1016/j.toxlet.2015.02.005

79 Chen, W. C. *et al.* Aryl hydrocarbon receptor modulates stroke-induced astrogliosis and neurogenesis in the adult mouse brain. *J Neuroinflammation* **16**, 187 (2019). https://doi.org/10.1186/s12974-019-1572-7

80 García-Lara, L., Pérez-Severiano, F., González-Esquivel, D., Elizondo, G. & Segovia, J. Absence of aryl hydrocarbon receptors increases endogenous kynurenic acid levels and protects mouse brain against excitotoxic insult and oxidative stress. *J Neurosci Res* **93**, 1423-1433 (2015). https://doi.org/10.1002/jnr.23595

81 Wiggins, B. G. *et al.* Endothelial sensing of AHR ligands regulates intestinal homeostasis. *Nature* (2023). https://doi.org/10.1038/s41586-023-06508-4

82 Major, J. *et al.* Endothelial AHR activity prevents lung barrier disruption in viral infection. *Nature* (2023). https://doi.org/10.1038/s41586-023-06287-y

83 Shah, K. *et al.* Cell-intrinsic Aryl Hydrocarbon Receptor signalling is required for the resolution of injury-induced colonic stem cells. *Nat Commun* **13**, 1827 (2022). https://doi.org/10.1038/s41467-022-29098-7

84 Arshadi, C., Günther, U., Eddison, M., Harrington, K. I. S. & Ferreira, T. A. SNT: a unifying toolbox for quantification of neuronal anatomy. *Nat Methods* **18**, 374-377 (2021). https://doi.org/10.1038/s41592-021-01105-7

85 Marcolino, A. M. *et al.* Assessment of functional recovery of sciatic nerve in rats submitted to low-level laser therapy with different fluences. An experimental study: laser in functional

recovery in rats. *J Hand Microsurg* **5**, 49-53 (2013). https://doi.org/10.1007/s12593-013-0096-0

86 Li, Y. *et al.* Macrophages facilitate peripheral nerve regeneration by organizing regeneration tracks through Plexin-B2. *Genes & development* **36**, 133-148 (2022). https://doi.org/10.1101/gad.349063.121

87 Martin, M. Cutadapt removes adapter sequences from high-throughput sequencing reads. *EMBnet.journal* **17**, 3 (2011). https://doi.org/10.14806/ej.17.1.200

88 Langmead, B. & Salzberg, S. L. Fast gapped-read alignment with Bowtie 2. *Nat Methods* **9**, 357-359 (2012). https://doi.org/10.1038/nmeth.1923

89 Danecek, P. *et al.* Twelve years of SAMtools and BCFtools. *Gigascience* **10** (2021). https://doi.org/10.1093/gigascience/giab008

90 Heinz, S. *et al.* Simple combinations of lineage-determining transcription factors prime cis-regulatory elements required for macrophage and B cell identities. *Mol Cell* **38**, 576-589 (2010). https://doi.org/10.1016/j.molcel.2010.05.004

91 Iqbal, A. *et al.* Flaski (3.12.2). *Zenodo* (2022). https://doi.org/10.5281/zenodo.7329954

92 Subramanian, A. *et al.* Gene set enrichment analysis: a knowledge-based approach for interpreting genome-wide expression profiles. *Proc Natl Acad Sci U S A* **102**, 15545-15550 (2005). https://doi.org/10.1073/pnas.0506580102

93 Krämer, A., Green, J., Pollard, J. & Tugendreich, S. Causal analysis approaches in Ingenuity Pathway Analysis. *Bioinformatics* **30**, 523-530 (2014). https://doi.org/10.1093/bioinformatics/btt703

94 Chen, E. Y. *et al.* Enrichr: interactive and collaborative HTML5 gene list enrichment analysis tool. *BMC Bioinformatics* **14**, 128 (2013). https://doi.org/10.1186/1471-2105-14-128

95 Kuleshov, M. V. *et al.* Enrichr: a comprehensive gene set enrichment analysis web server 2016 update. *Nucleic Acids Res* **44**, W90-97 (2016). https://doi.org/10.1093/nar/gkw377

96 Dreos, R., Ambrosini, G., Périer, R. C. & Bucher, P. The Eukaryotic Promoter Database: expansion of EPDnew and new promoter analysis tools. *Nucleic Acids Res* **43**, D92-96 (2015). https://doi.org/10.1093/nar/gku1111

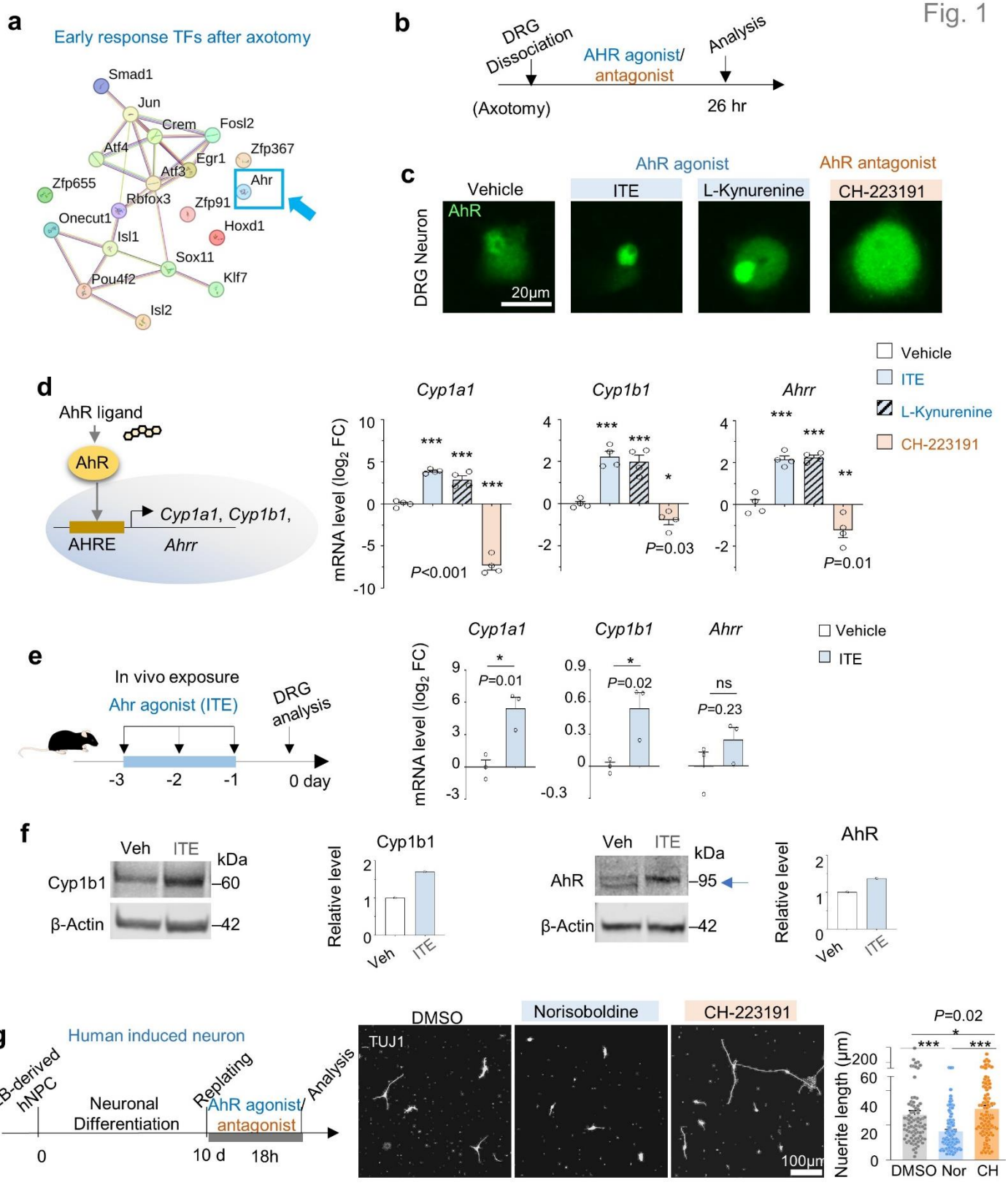

Figure 1. DRG neurons are responsive to ligand-mediated AhR signaling.

a. STRING protein-protein interaction network analysis revealed absence of known signaling link of AhR with other regeneration-associated TFs identified in our previous study (Zou et al. 2009) [1].

b. Schematic of primary DRG neuron cultures treated with AhR agonist or antagonist (or vehicle) and analyzed at 26 hr after plating. Note that axotomy (conditioning lesion) occurs during dissociation.

c. Representative IF images show changes of cytoplasm-nuclear shuttling of AhR in response to AhR agonists (ITE, 25 μM; L-Kynurenine, 25 μM) or AhR antagonist CH-223191 (25 μM).

d. Left, diagram of ligand-mediated AhR activation to induce canonical target genes through AHR response element (AHRE). Right, qRT-PCR results of AhR target genes normalized to housekeeping gene *Hprt* in primary DRG neurons with different treatments. n=4 independent DRG neuron cultures per group. Data represent mean ± SEM. One-way ANOVA with Dunnett's multiple test correction. ***P<0.001.

e. Left, experimental paradigm of adult mice receiving AhR agonist ITE (10 mg/kg; i.p, 3 daily injections) or vehicle (DMSO), followed by DRGs analysis 1 day later. Right, qRT-PCR results of gene expression of AhR canonical target genes normalized to *Hprt* in DRG from vehicle- or ITE-treated mice. n=3 independent L4-6 DRG samples from 3 mice. Data represent mean ± SEM. Unpaired two-tailed Student's *t*-test.

f. Western blots and quantifications of Cyp1b1 and AhR in DRG from vehicle- or ITE-treated mice. Arrow: electrophoretic mobility shift of AhR in DRGs from ITE-treated mice.

g. Left, experimental schematic of AhR agonist or antagonist stimulation of human induced neurons (from hESC via neuronal differentiation of embryoid body (EB) and human neuroprogenitor cells (hNPC)). Middle, representative IF images for TUJ1 of induced neurons after replating. Right, quantifications of neurite length. n=83-106 cells. Data represent mean ± SEM. One-way ANOVA with Dunnett's multiple test correction.

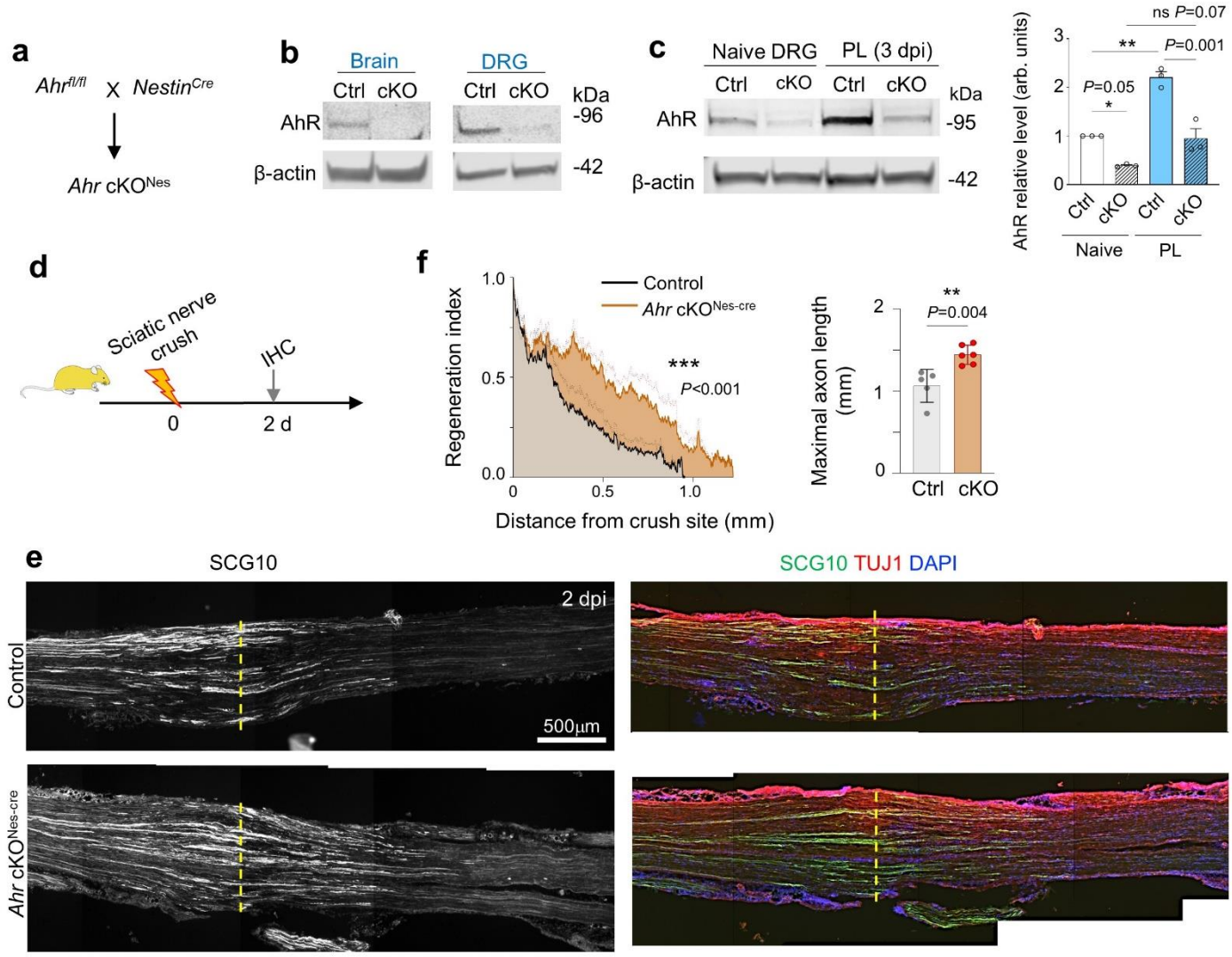

Figure 2. AhR deletion enhances axon regeneration after sciatic nerve injury.

a. Diagram of generating *Ahr* cKO$^{Nes\text{-}cre}$ mice by breeding *Ahr* floxed mice with Nestin-Cre allele.

b. Western blots show depletion of AhR in brain and DRGs from cKO^{Nes} mice. β-actin served as loading control.

c. Western blots and quantifications show expression of AhR in naive and conditioned DRG (3 dpi after PL) from *Ahr* cKO$^{Nes\text{-}cre}$ relative to control (Ctrl) mice. β-actin served as loading control. ***P<0.001. n=3 independent samples from 3 mice, each from pooled L4-L6 DRGs. Data represent mean ± SEM. Two-way ANOVA with Bonferroni multiple test correction.

d-f. Paradigm (d) of sciatic nerve crush injury and axon regeneration analysis by immunofluorescence (IF) at 2 dpi. IF images (e) and quantifications (f) show enhanced axon regrowth (SCG10^{+}) in *Ahr* cKO$^{Nes\text{-}cre}$ mice compared to littermate controls at 2 dpi (TUJ1 as general axon marker; DAPI for nuclear staining). Dashed lines denote crush center (based on highest immunointensity of SCG10). n=5 control and 6 cKO mice per group. Data represent mean ± SEM. Unpaired two-tailed Student's *t*-test for

maximal axon length. Two-way ANOVA for regeneration index.

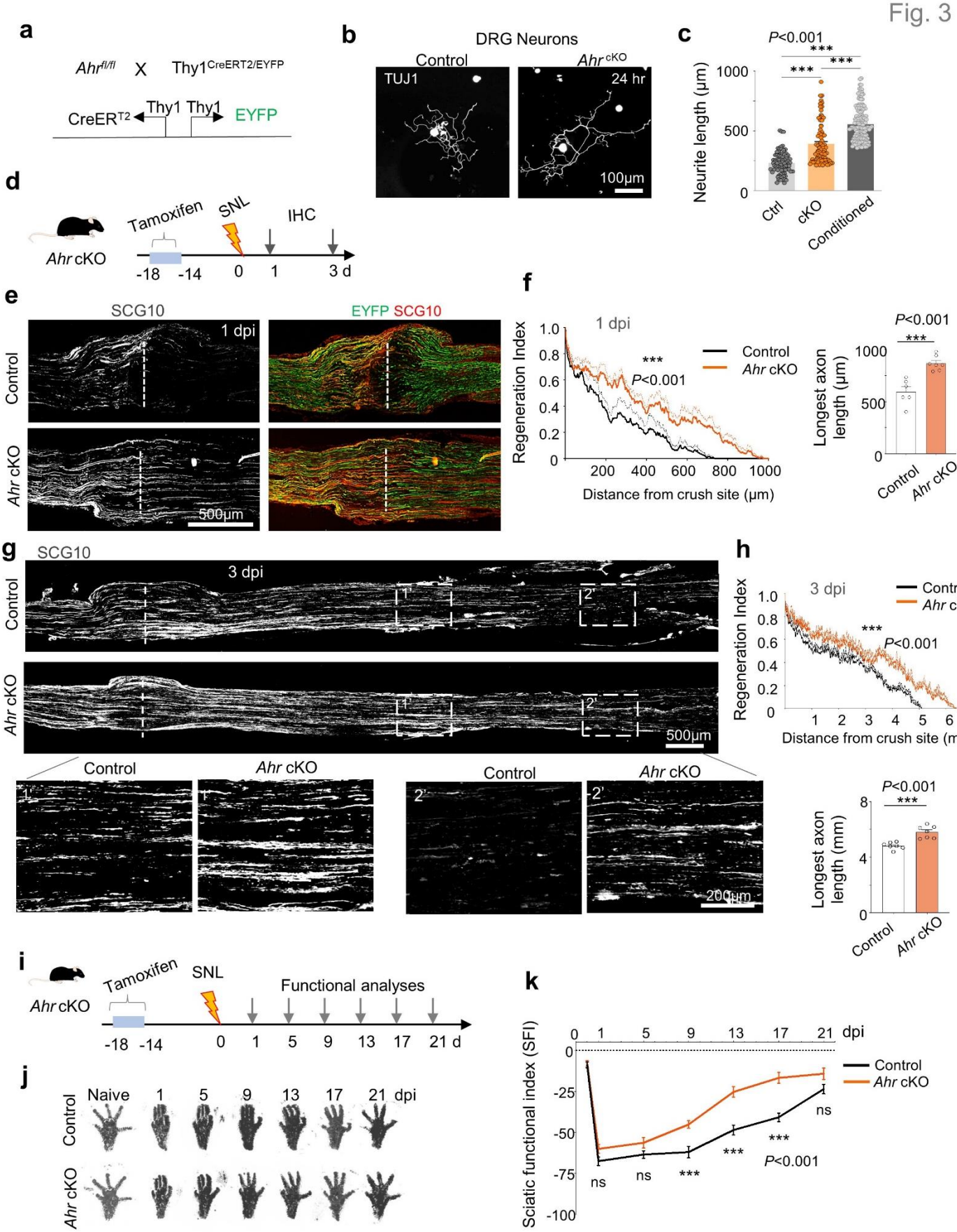

Figure 3. Neuronal *Ahr* cKO enhances axon regeneration and improves functional recovery.

a. Diagram of crossing *Ahr*$^{fl/fl}$ allele to Thy1$^{CreERT2/EYFP}$ transgenic line expressing tamoxifen inducible CreER and EYFP (driven by bidirectional Thy1 promoter).

b, c. Representative IF images (b) and quantification (c) of neurite outgrowth (TUJ1^{+}) of primary DRG neurons from *Ahr*$^{fl/fl}$ Thy1$^{CreERT2/EYFP}$ (*Ahr* cKO) or littermate controls after tamoxifen injection (100 mg/kg; i.p., five daily injection) 14 days prior. n=81, 81, and 149 for control, *Ahr* cKO, or pre-conditioned DRG neurons, respectively, collected from n=2 mice per genotype. Bar graphs represent mean ± SEM. One-way ANOVA with Dunn's multiple comparisons test.

d. Experimental paradigm. Tamoxifen (100 mg/kg; i.p., 5 daily) was administered 14 days prior to sciatic nerve crush lesion (SNL). Axon regeneration was assessed by IF for SCG10 at 1 and 3 dpi.

e-h. Representative IF images (e, g) and quantifications (f, h) of SCG10^{+} axons traversing lesion center (dashed lines) in sciatic nerve at 1 dpi or 3 dpi, respectively. Magnified images for 3 dpi are shown below. n=6 control and n=7 cKO mice per group. Regeneration index, two-way ANOVA with Bonferroni multiple test correction; longest axon length distal to lesion center, unpaired two-tailed Student's *t*-test. Data represent mean ± SEM.

i. Experimental scheme of motosensory assessment, from baseline before injury until 21 dpi. Sciatic nerve crush lesion (SNL) was performed 14 days after tamoxifen injections (100 mg/kg; i.p., 5 daily).

j, k. Representative hindlimb pawprints (j), at baseline and different time points after SNL, collected for measurement of sciatic functional index (k). n=5 mice per group. Data represent mean ± SEM. Two-way ANOVA with Bonferroni multiple test correction. ***P<0.001.

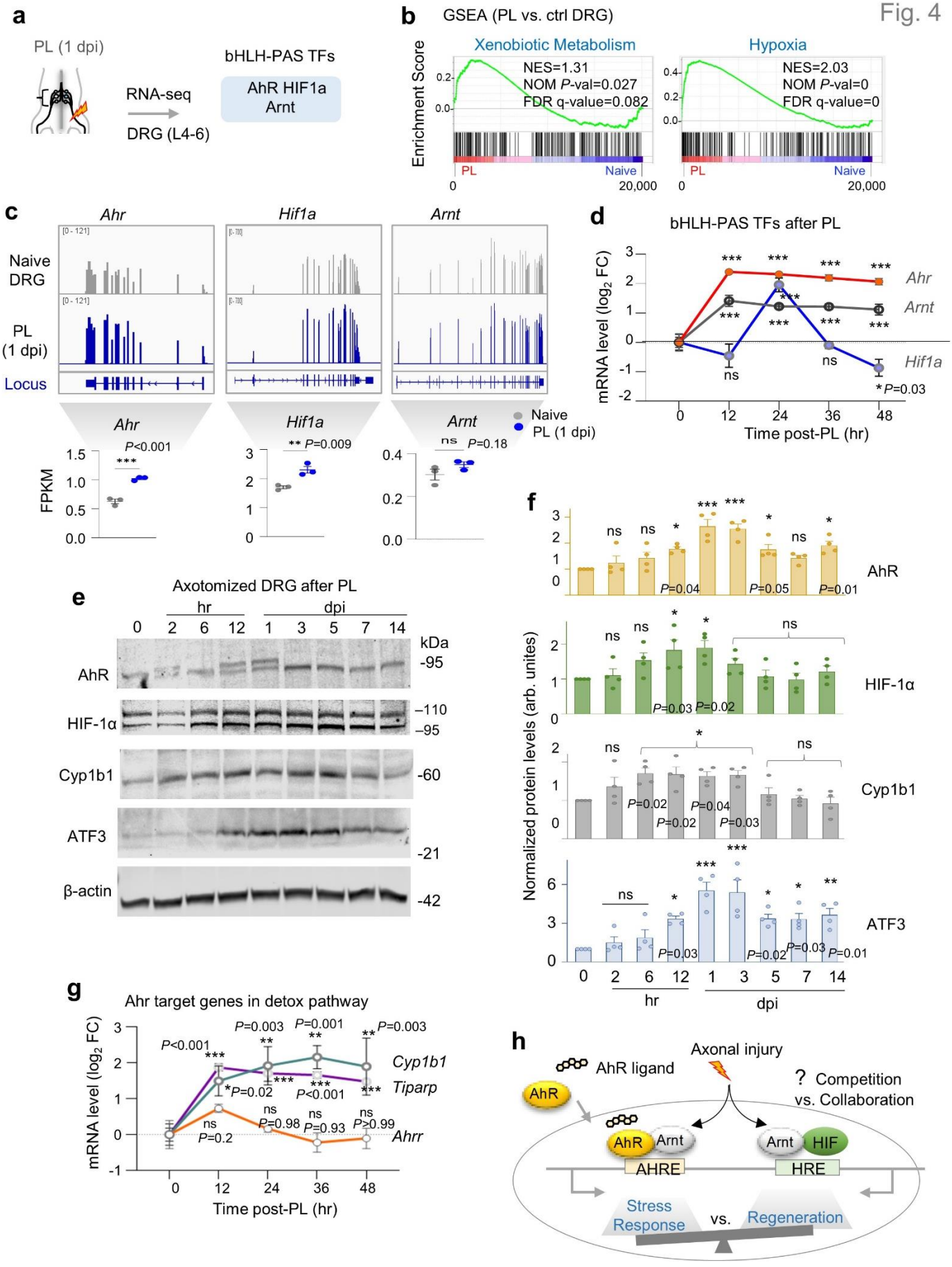

Figure 4. Peripheral lesion of DRG results in early induction of AhR and HIF-1α.

a. Diagram of RNA-seq analysis of lumbar 4-6 DRGs at 1 day after PL as compared to uninured (naive) DRGs. bHLH-TFs were denoted in blue.

b. GSEA shows enrichment of Xenobiotic metabolism and Hypoxia in injured DRG at 1 dpi as compared to naive DRG (~20,000 genes from RNA-seq data, comparing PL vs. naive). NES, normalized enrichment score; FDR, false discovery rate.

c. Top, RNA-seq read tracks of the indicated TFs. Bottom, graphs showing RNA-seq FPKM (fragments per kilobase of transcript per million reads) values of the genes from n=3 independent DRG samples per condition. Unpaired two-tailed Student's *t*-test.

d. Time-course qRT-PCR analyses of *Ahr*, *Arnt*, and *Hif1a* expression at early time points after PL, normalized to housekeeping gene *Hprt*. Data represent mean ± SEM. n=3 independent samples, each pooled from L4-L6 DRGs from n=3 mice per group. One-way ANOVA with Dunnett's multiple test correction. ***P<0.001; ns, not significant.

e, f. Western blots (e) and quantifications (f) of gene expression in DRG at different time points after PL relative to no injury (β-actin as loading control). n=4 independent DRG samples from 4 mice per time point. Bar graphs represent mean ± SEM. One-way ANOVA with Dunnett's multiple test correction.

g. Time course qRT-PCR analyses of canonical AhR target genes in DRG after PL relative to no injury (normalized to housekeeping gene *Hprt*). Data represent mean ± SEM. n=3 independent samples from 3 mice per group, each pooled from L4-L6 DRGs. One-way ANOVA with Dunnett's multiple test correction.

h. Schematic model of competitive vs. collaborative interaction between AhR and HIF pathways to regulate shared or distinct injury response or regeneration-associated genes.

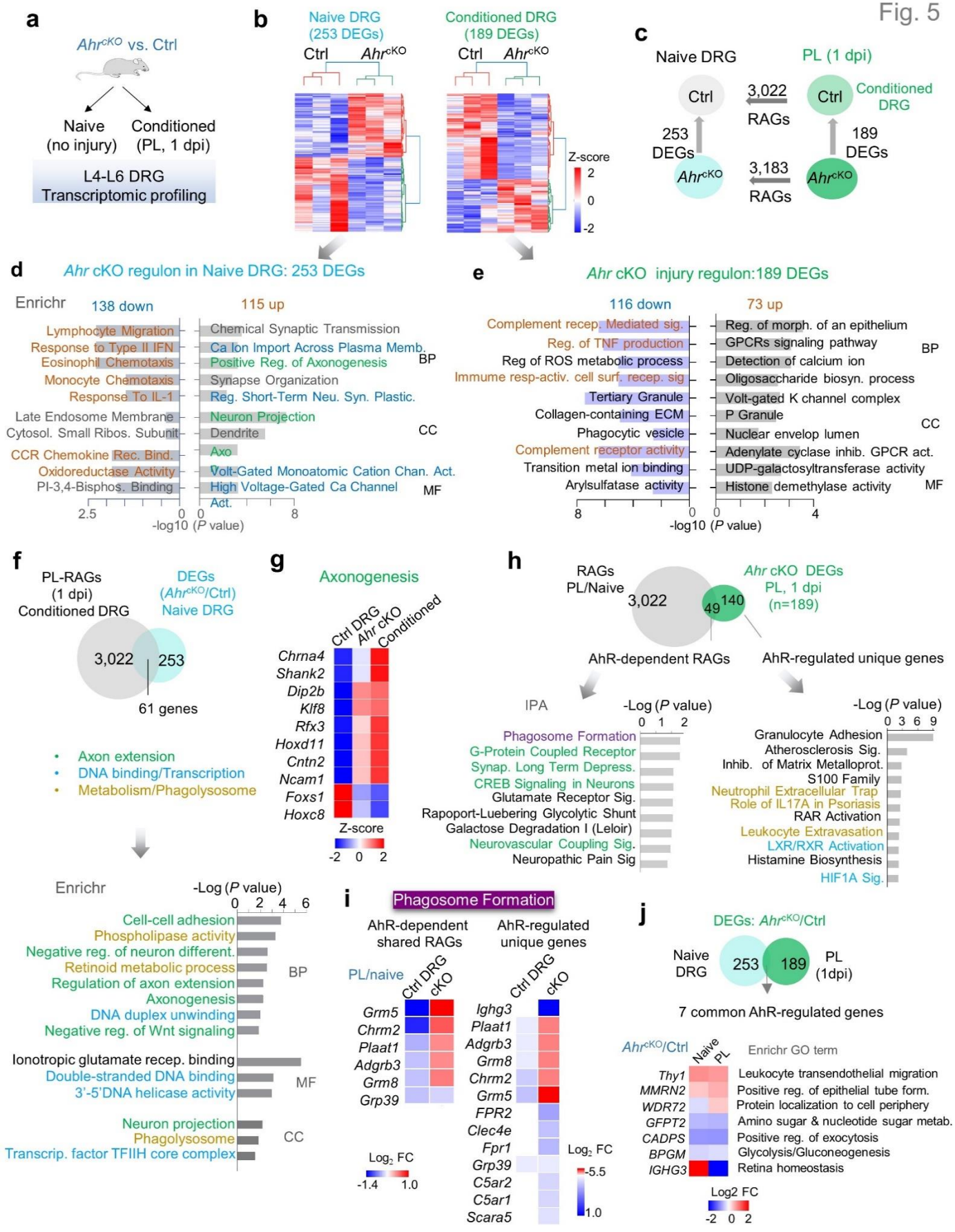

Figure 5. AhR cKO mimics conditioning lesion in initiating axonogenesis gene program while

suppressing stress response.

a. Experimental paradigm of RNA-seq of DRG from *Ahr*^{cKO} vs. littermate controls (n=3) in naive state or after PL at 1 dpi.

b. Heatmaps of hierarchically clustered differentially expressed genes (DEGs) in *Ahr*^{cKO} vs. control DRG in naive or axotomized state (triplicate each, cutoff: $\log_2$ FC >0.25 and P <0.05).

c. Summary diagram of 4-way comparison of DEGs in control or *Ahr*^{cKO} DRGs in naive or axotomized state at 1dpi. PL-RAGs in control DRG (n=3,022) were previously reported in Halawani et al. 2023.

d, e. Enrichr pathway analysis of up- and downregulated DEGs (*Ahr* cKO/Ctrl) in naive DRG (d) or axotomized DRG at 1 dpi (e). BP, biological process; CC, cellular component; MF, molecular function.

f. Top, Venn diagram showing overlap of genes between PL-RAGs after conditioning lesion at 1 dpi and AhR regulon in naive DRG. Bottom, top enriched ontologies (by Enrichr) of 61 overlapping genes.

g. Heatmap of relative expression of genes of the gene ontology (GO) terms Neuro-projection, Axonogenesis, and Axon guidance (part of the 61 overlap RAGs).

h. Top, Venn diagram showing 49 overlapping genes between PL-RAGs (PL/naive) and AhR injury regulon at 1 dpi (*Ahr*^{cKO}/Ctrl) and 140 unique AhR-dependent genes. Bottom, IPA of top canonical pathways of shared or unique genes.

i. Heatmaps of transcriptional changes of genes of the Phagosome Formation IPA canonical pathway in response to PL in *Ahr*^{cKO} vs. control DRG.

j. Top, Venn diagram showing only 7 common genes between *Ahr* cKO regulon in naive and injured DRG. Bottom, heatmap of transcriptional changes of these genes in different states of DRG. Gene name and GO terms are listed.

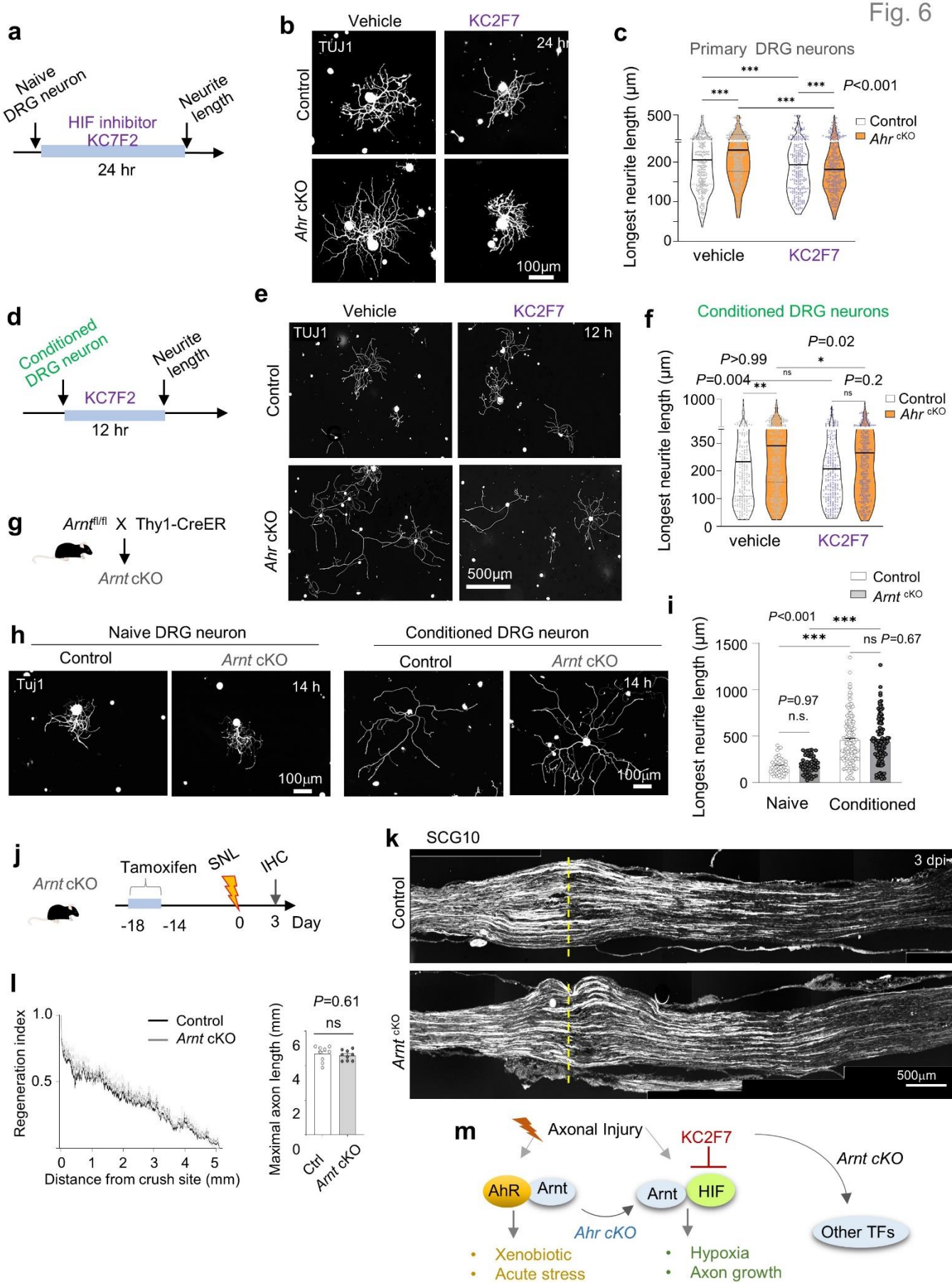

Figure 6. Growth promoting effect of *Ahr* deletion requires HIF1α.

a-f. Neurite outgrowth assay of primary DRG neurons (a-c) or conditioned DRG neurons with peripheral axotomy 3 days prior (d-f). Experimental schemes: DRG neurons treated with HIF1α inhibitor KC2F7 (10 μM) and examined at 24 hr after plating for primary DRG neurons (a) or at 12 hr for conditioned DRG neurons (d). Representative IF images for TUJ1 (b, e) and quantifications of neurite outgrowth (c, f). Violin plots of n=250-408 neurons for each condition. Black line denotes median. Two-way ANOVA followed by Bonferroni's multiple comparison test.

g. Experimental scheme for generation of *Arnt* cKO (*Arnt*$^{fl/fl}$ Thy1-CreERT2/EYFP) mice.

h, i. Representative IF images for TUJ1 (h) of naive or conditioned DRG neurons from *Arnt* cKO or control mice at 14 hr post-seeding. Quantifications (i) from n=51-52 neurons for naive and n=122-157 for conditioned DRG neurons from n=5 mice per genotype. Bar graphs represent mean ± SEM. Two-way ANOVA followed by Bonferroni's multiple comparison test. Significance.

j-l. Experimental paradigm: sciatic nerve crush lesion (SNL) was performed 14 days after tamoxifen injection (100 mg/kg, i.p., 5 daily) and axon regrowth analyzed at 3 dpi (j). Representative IF images (k) and quantification of axon regeneration (SCG10^{+}) at 3 dpi (l). Dashed lines: lesion center. n=9 mice per genotype. Two-way ANOVA for regeneration index. Unpaired two-tailed Student's *t* test for maximal axon length.

m. Working model of Ahr and HIF competition for heterodimerization partner Arnt.

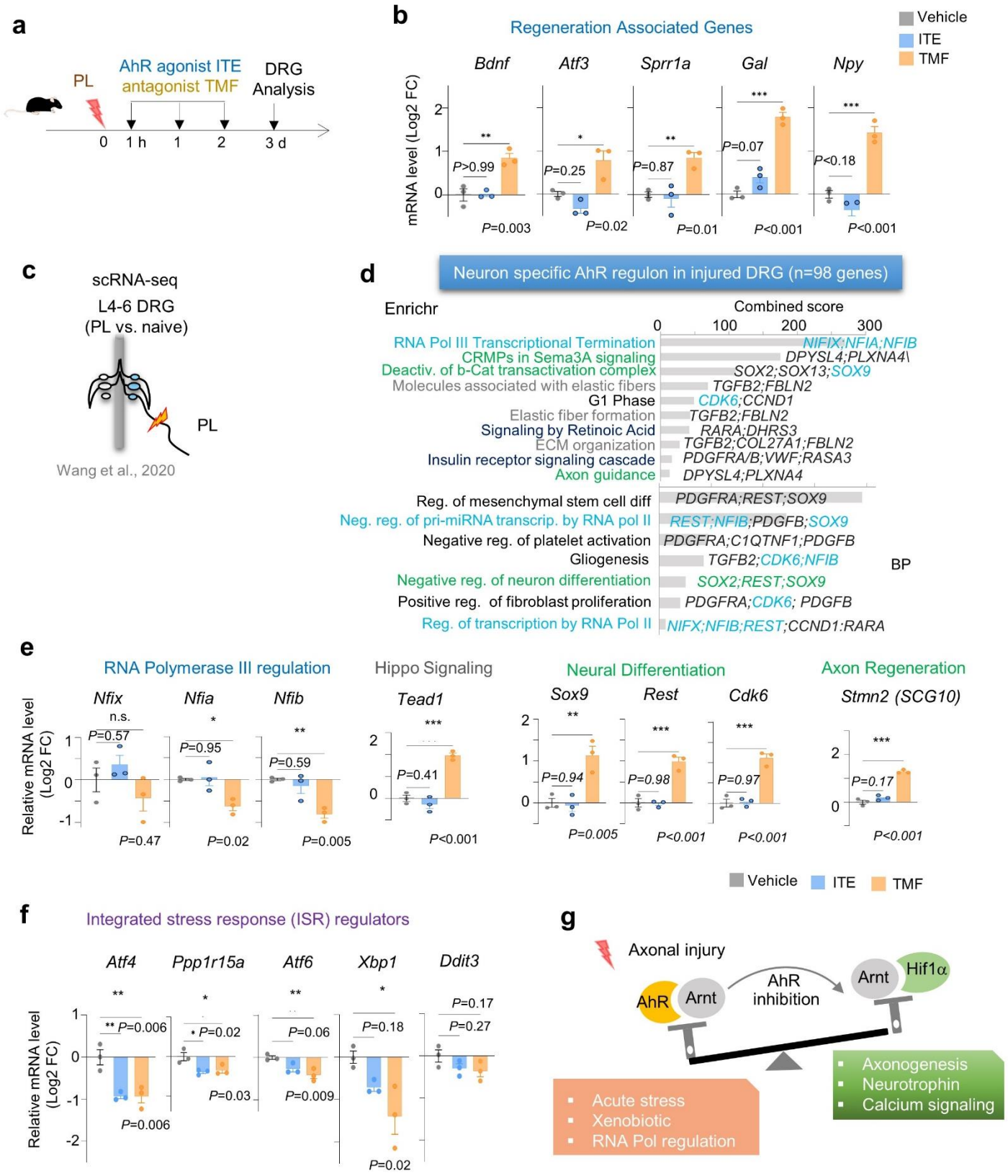

Figure 7. Pharmacological attenuation of AhR activation impacts RNA Polymerase III regulation and ISR in injured DRG.

a. Experimental paradigm of in vivo injection of AhR agonist (ITE, 10 mg/kg; i.p.), antagonist (TMF, 10 mg/kg; i.p.), or vehicle (DMSO) after sciatic nerve crush injury. DRGs were collected for analysis at 3 dpi.

b. qRT-PCR results (normalized to housekeeping gene *Hprt*) demonstrating augmented induction of RAGs with AhR antagonist TMF after PL. Data represent mean ± SEM. n=3 independent samples, each pooled from L4-L6 DRGs from 3 mice per group. One-way ANOVA with Dunnett's multiple test correction.

c. Schematic of scRNA-seq of axotomized DRG after sciatic nerve injury relative to no injury DRG (Wang et al. 2021) [2].

d. Enrichr analysis reveals top enriched pathways for the 98 predicted DRG neuron specific AhR regulon after PL from scRNA-seq. BP, biological process.

e. qRT-PCR analysis of genes in the indicated Enrichr GO terms shown above. Results were normalized to housekeeping gene *Hprt*. Data represent mean ± SEM. n=3 independent samples, each pooled from L4-L6 DRGs from 3 mice per group. One-way ANOVA with Dunnett's multiple test correction.

f. qRT-PCR analysis of gene expression of ISR regulators (normalized to housekeeping gene *Hprt)*. Data represent mean ± SEM. n=3 independent samples, each pooled from L4-L6 DRGs from 3 mice per group. One-way ANOVA with Dunnett's multiple test correction.

g. Diagram of working model of the role of AhR in balancing neural injury and regenerative responses.

References in Figure Legends

1 Zou, H., Ho, C., Wong, K. & Tessier-Lavigne, M. Axotomy-induced Smad1 activation promotes axonal growth in adult sensory neurons. *J Neurosci* **29**, 7116-7123 (2009). https://doi.org/10.1523/jneurosci.5397-08.2009

2 Wang, K. *et al.* Single-cell transcriptomic analysis of somatosensory neurons uncovers temporal development of neuropathic pain. *Cell Res* **31**, 904-918 (2021). https://doi.org/10.1038/s41422-021-00479-9